

# Comparison of volumetric-modulated arc therapy and intensity-modulated radiation therapy prostate cancer plans accounting for cold spots

ジョン, ティ, タオ, ウィン

<https://doi.org/10.15017/2348709>

---

出版情報 : Kyushu University, 2019, 博士 (保健学), 課程博士  
バージョン :  
権利関係 :



# Doctoral Thesis

Comparison of volumetric-modulated arc therapy and intensity-modulated radiation therapy prostate cancer plans accounting for cold spots

Division of Medical Quantum Science, Department of Health Sciences  
Graduate School of Medical Sciences, Kyushu University

Student ID: 3MD15509S

Tran Thi Thao Nguyen



# Comparison of volumetric-modulated arc therapy and intensity-modulated radiation therapy prostate cancer plans accounting for cold spots

Department of Health Sciences

3MD15509S

Tran Thi Thao Nguyen

**Purpose:** To compare dosimetric indices of volumetric-modulated arc therapy (VMAT) with intensity-modulated radiation therapy (IMRT) accounting for cold spots in prostate cancer plans.

**Materials and methods:** IMRT plans were retrospectively generated from 30 prostate cancer patients with 10 cases for each risk group, who received VMAT plans. The mean, maximum, and minimum doses and conformity and homogeneity indices were evaluated for planning target volume (PTV) and the mean dose and V20 to V70 for organs at risk (OAR) including the rectum, bladder, right and left femoral heads, and rectum overlapped with PTV (ROP) regions. The numbers and volume percentages of cold spots within PTVs and ROP regions were measured using in-house software. Three-dimensional probabilistic distributions of cold spots were generated using a centroid matching technique for visualization and analysis.

**Results:** There was a statistically better dose conformity in the PTV, rectum, and bladder dose-sparing in VMAT compared to that in the IMRT plans, whereas VMAT plans had statistically worse target dose homogeneity and right and left femoral head dose-sparing than those of the IMRT plans. The average volume percentage of cold spots per PTV for the VMAT plans was  $4.37 \pm 2.68\%$ , which was smaller than the  $5.72 \pm 1.84\%$  observed for IMRT plans ( $P = 0.007$ ). The volume percentage of cold spots per ROP for the VMAT plans did not significantly differ from those for the IMRT plans.

**Conclusions:** Compared with IMRT plans, the VMAT plans achieved better PTV dose conformity, OAR dose-sparing, and smaller cold spots in the treatment of prostate cancer.

**Keywords:** Prostate cancer · cold spot · VMAT · IMRT · probabilistic distribution

## 和文レポート

**タイトル：**前立腺癌治療計画における IMRT と VMAT のコールドスポットの比較

**目的：**本研究では、前立腺癌治療計画における強度変調放射線治療(IMRT)と強度変調回転放射線治療(VMAT)の低線量領域(コールドスポット)の比較を目的とした。

**方法：**本研究では、VMATで治療された30症例の治療計画とその治療計画から再立案されたIMRTの治療計画で比較を行った。また、リスク臓器(OAR)として直腸、膀胱、左右大腿骨頭、直腸と計画標的体積(PTV)の重なり領域(ROP領域)と定義し、治療計画の線量評価指標として、PTVに対しては平均線量、最大線量、最低線量、conformity index (CI), homogeneity index (HI)を用い、OARに対しては平均線量、V20-V70を用いた。また、自作ソフトウェアを用いて、PTVおよびROP領域の内のコールドスポットの数と体積を推定した。さらに、可視化と分析ため、重心マッピング法を用いてコールドスポットの三次元確率分布を作成した。

**結果：**IMRTと比較して、VMATの治療計画はPTVのCIとOAR(直腸、膀胱)の線量に関して有意に優れていた。PTVのHIと左右大腿骨頭の線量評価指標に関してVMATはIMRTより劣っていた。また、IMRTとVMAT間のPTVに対するコールドスポットの全症例の平均体積の割合は、それぞれ $0.572 \pm 0.184$ 及び $0.437 \pm 0.268$  ( $P = 0.007$ )だった。また、ROP領域に対するコールドスポットの平均体積の割合には有意差がなかった。

**結論：**前立腺癌の放射線治療において、IMRT と比較して、VMAT は PTV の CI、OAR の線量、コールドスポットの体積に関して優れていることが示された。

**キーワード：**前立腺癌;コールドスポット;強度変調放射線治療;強度変調回転放射線治療;確率分布

## Contents

Chapter 1 Introduction .....	1
1.1 Background .....	1
1.2 Purpose.....	5
Chapter 2 Basic theories of intensity-modulated radiation therapy and volumetric-modulated arc therapy .....	6
2.1 Intensity-modulated radiation therapy (IMRT).....	6
2.1.1 IMRT inverse treatment planning .....	6
2.1.2 Cost function.....	7
2.2 Volumetric-modulated arc therapy (VMAT).....	8
2.2.1 VMAT optimization.....	8
Chapter 3 Comparison of volumetric-modulated arc therapy and intensity-modulated radiation therapy prostate cancer plans accounting for cold spot .....	11
3.1 Clinical cases .....	11
3.2 Plan evaluation.....	15
3.4 3D PD of the probability and distributions of cold spots.....	18

3.5 Statistical analysis.....	19
3.6 Results.....	19
3.7 Discussion.....	30
Chapter 4 Conclusions .....	34
Acknowledgements.....	35
References.....	36
Achievements.....	41

## Abbreviations and keywords

Abbreviation	Full spelling	Explanation
VMAT	Volumetric-modulated Arc Therapy	A radiation technique which delivers radiation doses while varying the multileaf collimator motion, dose rate, and gantry rotation speed.
IMRT	Intensity-modulated Radiation Therapy	An advanced form of three-dimensional conformal radiotherapy which used multiple fixed angle radiation beams and non-uniform intensity of the radiation beams.
DVH	Dose-volume Histogram	A plot of a cumulative dose-volume frequency distribution which graphically summarizes the simulated radiation distribution within a volume of interest of a patient which would result from a proposed radiation treatment plan.
OAR	Organs at Risk	Non-target tissues that could suffer significant morbidity and might influence the treatment planning and/or the absorbed dose prescription if irradiated.
PTV	Planning Target Volume	A geometrical concept introduced to ensure that the prescribed dose will actually be delivered to all parts of the CTV with a clinically acceptable probability, despite geometrical uncertainties such as organ motion and setup variations, by adding margins surrounding the CTV.
ROP	Rectum-overlap PTV	The region in which the rectum overlaps with the PTV in prostate cancer radiation treatment.



## Chapter 1 Introduction

### 1.1 Background

Recently, prostate cancer is one of the most common malignant diseases in men worldwide, especially those in developed countries [Ferlay et al. 2015]. Prostate cancer is the seventh leading cause of cancer death in Japanese men [Kitazawa et al 2015]. Figure 1.1 illustrates several treatment options include prostatectomy, chemotherapy, hormonotherapy, and radiotherapy to treat prostate cancer patients.

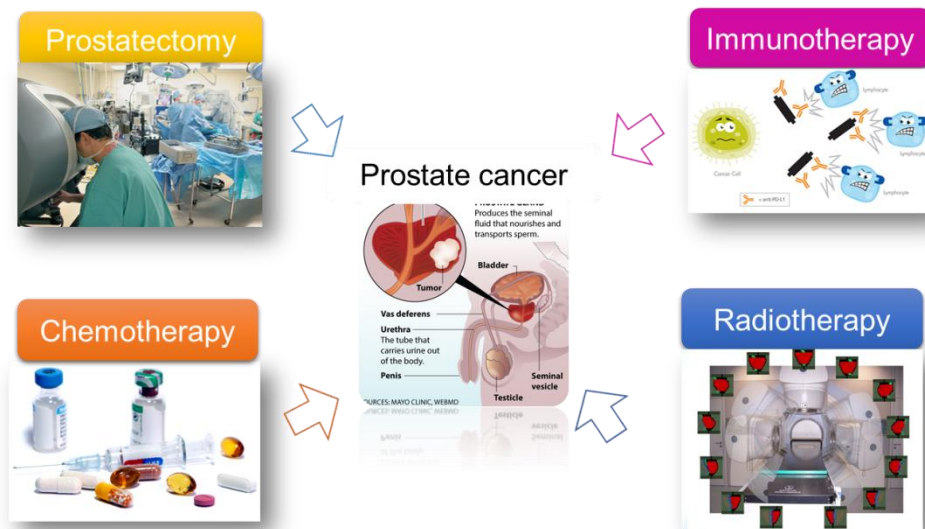


**Fig. 1.1** Illustration of treatment options for patient with prostate cancer.

There has been a significant increase in the number of prostate cancer patients treated with volumetric-modulated arc therapy (VMAT) and intensity-modulated radiation therapy (IMRT) in Japan [Ogawa et al. 2011] because of their lower risks of urinary and sexual dysfunctions. In static IMRT (step-and-shoot technique), a multileaf collimator (MLC) divides each radiation beam into a set of smaller segments of differing MLC shape to conform to and administer high doses to the tumor and improve sparing of normal tissue and organs at risk (OAR), resulting in the reduction of acute and late toxicities [King et al. 2000; Ezzell et al. 2003]. In dynamic IMRT (sliding window technique), multiple fixed angle

radiation beams and continuously moving MLC are used to modulate the intensity of each radiation beam [ICRU 83; Rana et al. 2013]. VMAT delivers radiation doses while varying the MLC motion, dose rate, and gantry rotation speed [Otto et al. 2008]. Figure 1.2 shows the arrangement of radiation beams for (a) VMAT and (b) IMRT in the representative axial computed tomography (CT) slices.

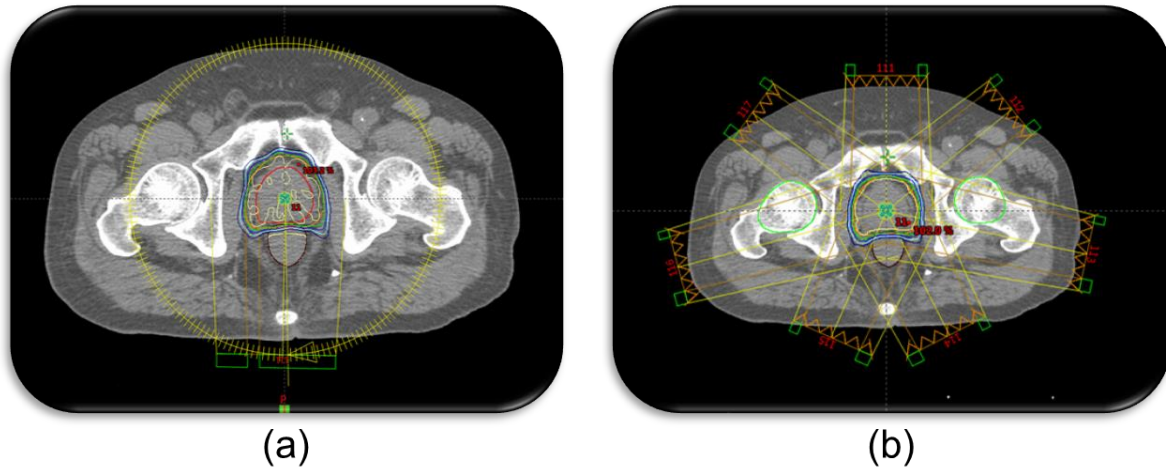


**Fig. 1.2** Representative axial computed tomography slices showing arrangement of radiation beams for (a) volumetric-modulated arc therapy and (b) intensity-modulated radiation therapy.

However, in VMAT and IMRT treatment plans, there are trade-offs in target coverage and OAR dose-sparing, which result in routine encountering of high dose (hot spots) and low dose (cold spots) regions in the planning target volume (PTV) [Jeraj et al. 2002; Mundt et al. 2005; Dogan et al. 2006; Bortfeld et al. 2008]. According to the study of Tomé et al. on the effect of a small volume of cold spots on TCP for solid tumors, one of the causes of the tumor recurrences is the occurrence of cold spots in target volume because cold spots could lead to the decrease of TCP [Tomé et al. 2002]. In order to focus on the tumor control, we deal only with cold spots in this study.

In general, cold spots are defined as volumes of tissue that receive doses less than an applicable percentage of the prescribed dose [Mundt et al. 2005]. We should use the definition of the cold spots for prostate cancer plans. However, to the best of our knowledge, at present there is no generally acceptable consensus regarding the magnitude, volume, and distribution for cold spots for most of cancer types, including prostate cancer. Therefore, we employed the trial guidelines of the Radiation Therapy Oncology Group (RTOG) H-0222 [Mundt et al. 2005] for this study, which provided recommendations including cold spots for head and neck cancer. The cold spots are defined as regions that receive doses lower than 93% of the prescribed dose within PTV [Mundt et al. 2005]. The total volume of cold spots should be  $< 1\%$  of the PTV [Mundt et al. 2005]. The locations of cold spots are important, because they should not be located within the gross tumor volume (GTV) and ideally should be at the periphery of the PTV, as far as from the GTV as possible [Mundt et al. 2005]. Therefore, it is essential to understand the distributions of the probability of the existence of cold spots and the distributions of the cold spots if they were to occur in radiation therapy plans. Several studies have shown that underdosing even small fractions of target volume can result in a reduction of tumor control probability (TCP), which would cause recurrences of tumors due to insufficient irradiation to PTV [Bortfeld et al. 2008; Tomé et al. 2002; Vora et al. 2013; Zaorsky et al. 2016]. Vora et al. evaluated the long-term control of the disease and chronic toxicities observed in patients treated with IMRT for prostate cancer [Vora et al. 2013]. The results of their study showed that local and distant recurrent rates of 5% and 8.6%, respectively. In addition, the nine-year biochemical control rates were 77.4% for low-risk patients, 69.6% for intermediate-risk patients, and 53.3% for high-risk patients who received IMRT [Vora et al. 2013].

The region in which the rectum overlapped with the PTV along the anterior wall is defined as the rectum-overlap PTV (ROP) region. Figure 1.3 illustrates the ROP region of a prostate cancer patient as determined by radiation oncologists.

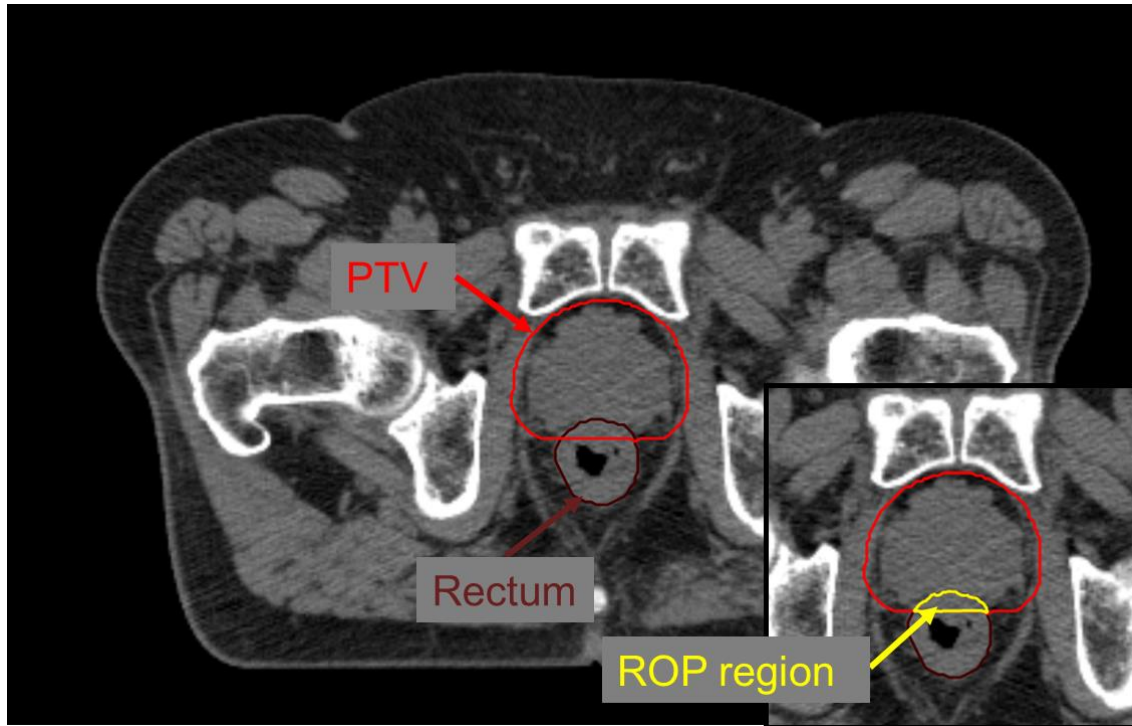


**Fig. 1.3** Illustration of the ROP region of a prostate cancer patient as determined by radiation oncologists. The yellow contour indicates a ROP region as viewed from the inferior-superior (IS) direction.

Cold spots in ROP regions may be associated with recurrences of tumors. Therefore, the investigation of cold spots in the ROP regions is necessary to understand how the magnitude, volume, and distribution of these low dose regions in VMAT and IMRT plans.

Several reports on VMAT and IMRT plans have been published [Palma et al. 2008, Wolff et al. 2009, Quan et al. 2012; Guckenberger et al. 2009; Kjaer et al. 2009; Yoo et al. 2009; Ost et al. 2011; Sze et al. 2012; Shaffer et al. 2009; Kopp et al. 2011]. Wolff et al. reported that both VMAT and IMRT yielded treatment plans of improved quality in comparison with three dimensional (3D)-conformal treatments by analyzing their dose

distributions with various dosimetric indices [Wolff et al. 2009]. Quan et al. evaluated the differences in plan qualities between VMAT and IMRT while considering the delivery time and the number of beams in IMRT [Quan et al. 2012]. However, to the best of our knowledge, no studies have compared VMAT and IMRT plans with respect to not only target dose conformity and homogeneity, rectum overlapped with PTV (ROP) dose-sparing and OAR (rectum, bladder, right and left femoral heads) dose-sparing but also the number, volume, and probabilistic distributions (PD) of cold spots in the PTV and ROP region in the treatment of prostate cancer.

## **1.2 Purpose**

The purpose of this study was to compare VMAT with IMRT, accounting for cold spots in prostate cancer plans. In this study, the mean, maximum, and minimum doses and conformity and homogeneity indexes were evaluated for the PTV; the mean dose and V20 to V70 for OAR including the rectum, bladder, right and left femoral heads, and ROP regions. In addition, the numbers and volume percentages of cold spots within PTVs and ROP regions were measured using in-house software. 3D PD of the probability and distributions of cold spots were generated using a centroid matching technique for their visualization and analysis.

## Chapter 2 Basic theories of intensity-modulated radiation therapy and volumetric-modulated arc therapy

### 2.1 Intensity-modulated radiation therapy (IMRT)

IMRT is one of commonly used methods to treat cancer in the field of radiation therapy. The initial developments on IMRT were evolved from the development of three-dimensional radiation therapy (3DCRT) in the 1980s [Perez et al. 1995]. IMRT has been implemented in clinical use since the late 1990s. The most important feature of this method is that the beam intensity of each radiation fixed beam is modulated so that a highly conformal dose is delivered to the target volume receives while the surrounding normal tissues and sensitive structures can be spared. In this section, the main concepts of IMRT will be presented as simple as possible. Firstly, let us try to clarify a main concept of the treatment planning in IMRT: inverse treatment planning.

#### 2.1.1 IMRT inverse treatment planning

IMRT uses the inverse treatment planning as mentioned above. The main concept of three dimensional (3D) dose distribution is indicated by the following equation [Mayles et al 2007, Webb 2005]

$$\mathbf{D} = M\mathbf{w}_i \quad (2.1)$$

where  $\mathbf{D}$  is a 3D dose distribution related to the set of beam-weights,  $M$  is the matrix linking each beam-space element to each dose-space element,  $\mathbf{w}_i$  is the vector of individual beam-weights,  $i$  is number of beams. The elemental entries into  $M$  depend on the physics of photon-tissue interaction and can be pre-calculated using Monte Carlo calculation or convolution and superposition algorithms.

The “inverse treatment planning” is that we can know the dose  $\mathbf{D}$  as the prescribed dose, and we also know  $M$  and we require to calculate the vector of individual beam-weights  $\mathbf{w}_i$ . The basic idea is that the computer investigates a range of options for pixel weights ( $\mathbf{w}_i$ ) then calculates the delivered dose based on the equation 2.1. Depending on whether the change in pixel weights makes the increase or decreases of the cost function, the change is either accepted or rejected based on an acceptable cost.

### 2.1.2 Cost function

Cost function is a measure of the quality of a plan, i.e. how good or bad a treatment plan is [Taqaddas et al. 2011]. The basic concept of the cost function,  $\mathbf{C}$ , will be explained in the following equation [Mayles et al 2007, Webb 2005]

$$\mathbf{C} = \sum_i^N I_i (\mathbf{D}_i - \mathbf{D}_i^p)^2 \quad (2.2)$$

where  $\mathbf{D}_i$  and  $\mathbf{D}_i^p$  are the delivered and prescribed doses to the  $i$ th voxel, respectively,  $N$  is number of voxels.  $I_i$  is the importance factor for the  $i$ th voxel.  $i$  is number of beams. The importance factor allows the planner to bias the plan selectively towards either the required dose in the PTV or that in the organs at risk [Webb 2005].

The iterative planning process might start off with empty beam. Given that the delivered dose  $\mathbf{D}_0$  will be zero, the starting cost function will be  $\mathbf{C} = \sum I_0 (\mathbf{D}_0^p)^2$ , and be at its highest. Now, considering offer a randomly small beam-weight to each beam element. After each addition, the cost function is recalculated. Changes to beam elements are accepted if they lead to a lower acceptable cost. In that ways, the delivered dose  $\mathbf{D}_i$  gradually builds up while the cost function value will decrease. Simultaneously the modulation of the beams will develop [Webb 2005]. In summary, such schemes attempt to minimize the difference between delivered and prescribed dose, reduce the cost function. In

other words, the iterative planning process is performed to reach the global minimum of the cost function or optimization.

## **2.2 Volumetric-modulated arc therapy (VMAT)**

VMAT was evolved from intensity modulated arc therapy (IMAT) proposed by Yu in 1995 [Yu 1995]. The idea of IMAT is to involve continuous gantry rotation with dynamic MLC motion to produce fluence modulation while the beam is on. Because the IMAT requires as many arcs as there are segments to be delivered, this technique has been computationally difficult in implementation in practice with respect to optimization of a treatment plan. In 2008, Otto overcame this difficulty and introduced a treatment planning algorithm for a single arc VMAT [Otto et al. 2008]. In this section, let us attempt to explain a main concept of optimization in the VMAT.

### *2.2.1 VMAT optimization*

VMAT also uses the inverse treatment planning as mentioned in Section 2.1.1. The cost function in the inverse treatment planning is based on dose-volume constraints [Otto et al. 2008]. The main purpose of optimization procedure is to minimize the cost of function to reach the global minimum of the cost function by using a computerised algorithm [Taqaddas et al. 2011]. There are two commonly used approaches in optimization. They are the stochastic approach and the deterministic approach [Chaos 2005]. The deterministic approach only allows a change in plan with a decrease value of the cost function. However, the stochastic approach also allows a change in plan with an increase of the cost function. There are a number of VMAT optimization algorithms used in practice, and some of them use simulated annealing algorithm.

Simulated annealing (SA) uses uphill and downhill changes to guarantees achieving the global minimum [Khan 2007]. According to Aquaddas [Aquaddas 2011], in this method,



one of the variables in the simulated annealing is randomly selected and its value is randomly increased or decreased by a small amount (grain). The grains represent the elemental changes in the beam-weight. At first, any changes of the variables are accepted and changes may be large to explore the solution space [Chao et al. 2005]. Then, the objective function is recalculated until the value of the cost function is negative, which means that the change lead to the decrease of the cost function, the change is accepted and the algorithm proceeds to the next iteration [Khan 2007, Mayles et al 2007]. In the case of the value of the objective function is positive, the change to the variable is rejected. However, there is an exceptional case which is a probability  $P$  given by an equation [Webb 2003, Taqaddas 2011]:

$$P = \exp(-\Delta V/kT) \quad (2.3)$$

where  $\Delta V$  is small fraction of cases  $V$ ,  $k$  is Boltzmann's constant,  $T$  is temperature. The variable  $kT$  is the controlling parameter which is used to decrease the probability  $P$  of accepting a wrong way (uphill) as long as the iteration process of searching continues. The temperature variable  $T$  is reduced gradually until the end of the iteration and only downhill changes are accepted in practice. This process enables the algorithm to come out of local minima into deeper minima that may be close to a global minimum [Taqaddas 2011]. Figure 2.1 illustrates the concept of simulated annealing by describing an analogy of a skier attempting to reach the foot (global minimum) of a slope (cost function) with snowbumps (local minima) [Mayles et al. 2007, Webb 2003]. In this figure, the hill represents the cost function. At the top of the hill, a starting line for the skier refers to the initial conditions when the cost function (slope) is high. The skier moves down the hill, i.e. the cost function begins to decrease. The purpose of the skier is moves down the hill to reach a foot of the hill (i.e. a global minimum) by avoiding to be trapped in any small snow bumps on the way of downhill (i.e. local minima). This purpose is achieved as the skier has to pass through downhill (i.e.

accepting a decrease) but also the small uphill changes (i.e. accepting a small decrease) in the slope (the cost function).

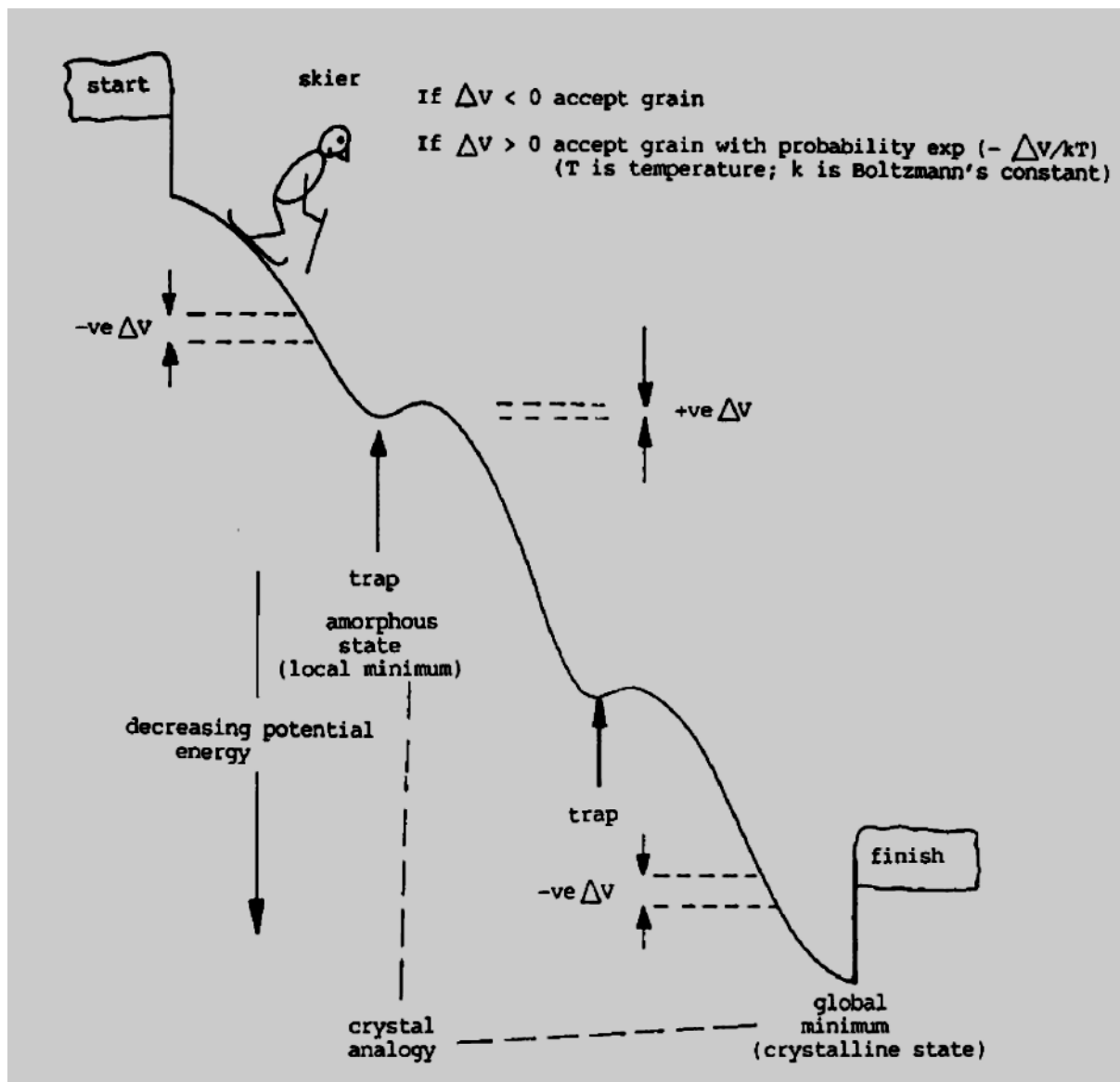


**Fig. 2.1** An illustration of the concept of simulated annealing (SA) algorithms by describing an analogy of a skier attempting to reach the foot (global minimum) of a slope (cost function) with snowbumps (local minima) [Mayles et al. 2007, Webb 2003].

## **Chapter 3 Comparison of volumetric-modulated arc therapy and intensity-modulated radiation therapy prostate cancer plans accounting for cold spot**

### **3.1 Clinical cases**

This study was performed under the approval of the institutional review board of our hospital. Thirty patients (median age: 72 years; range: 56-87 years; stage: T1-T3a) treated with VMAT for prostate cancer were selected for this study. These cases included 10 low-risk patients, 10 intermediate-risk patients, and 10 high-risk patients. The reason for using three risk categories is that the magnitude, volume, and distribution of cold spots within the PTVs may depend on the contours of 3 risk clinical target volumes (CTVs). The low-, intermediate-, and high-risk CTVs were defined as containing only the prostate, prostate plus 1 cm proximal seminal vesicles, and prostate plus 2 cm proximal seminal vesicles, respectively [Boehmer et al. 2006; Hayden et al. 2010]. PTV margins (internal and set-up margins) were added as 5 mm in posterior direction to spare additional rectal tissue from receiving radiation dose and 8 mm in other directions. The median volumes of the PTVs with its range were 101.62 cc (52.35 – 132.73 cc) for the low-risk group, 106.87 cc (75.99 – 159.25 cc) for the intermediate-risk group, 97.45 cc (75.59 – 137.63 cc) for the high-risk group, and 103.78 cc (52.35 – 159.25 cc) for all risk groups. The volumes (means  $\pm$  SDs) of the PTVs were  $96.22 \pm 22.98$  cc for the low-risk group,  $111.85 \pm 22.42$  cc for the intermediate-risk group,  $100.44 \pm 21.18$  cc for the high-risk group, and  $102.44 \pm 23.16$  cc for all risk groups.

IMRT plans were retrospectively generated from the 30 prostate cancer patients in three risk groups who received VMAT plans with a prescribed dose of 76 Gy in 38 fractions. The dose calculations for both techniques utilized an anisotropic analytical algorithm (AAA) [Bragg et al. 2008], with a dose calculation grid size of 2.5 mm and 10-MV photon beam, which was the algorithm implemented in the Varian Eclipse, version 10.0, treatment planning system. In plans for both VMAT and IMRT in our hospital, the mean dose within the PTV

was set as 100% of the prescribed dose [Michalski et al. 2004]. For the rectum, 65, 70, and 76 Gy covered less than 25%, 20%, and 3% of the volume, respectively. For the bladder, 40 and 70 Gy covered less than 60% and 35% of the volume, respectively. For the ROP, the average dose ranged from 90% to 95% of the prescribed dose. For the right and left femoral heads, the maximum dose was less than 50 Gy. Dose criteria in our institute follow the RTOG 0126 guideline [Michalski et al. 2004]. However, the OAR dose criteria were set as threshold values lower than these of RTOG 0126 due to a concern of reducing toxicity to OAR. Optimization parameters and their weightings (priorities) for VMAT and IMRT plans were summarized in Table 1.

**Table 1.** Optimization parameters and their weightings (priorities) for VMAT and IMRT plans.

Structure	Volume (%)	Dose (Gy)	Priority
CTV	100	76	90-98
Rectum_O	0	36-38	30-90
	30	20	40-65
	70	10	50
ROP	0	69-73	30-60
	100	68-70	50-80
PTV_Rectum	0	74-78	80-100
	100	75-77	70-100
Bladder	30	40	50
Rectum	0	68-70	50-80
Large bowel	0	45-60	60
	40	25	50

CTV: clinical target volume; PTV: planning target volume; Rectum\_O: rectum minus PTV with extra 5-mm margin; PTV\_Rectum: PTV minus rectum; ROP: rectum overlapped with PTV.

The VMAT plans consisted of a single arc starting at a gantry angle of 179° and stopping at a gantry angle of 181° in the counter-clockwise direction (Varian International Electrotechnical Commission [IEC] scale). The collimator was set to 30°. From the VMAT optimization, a series of MLC segments for each arc field was generated. One MLC segment formed an aperture shape from a beam at every 2 gantry positions, which translated to 178 segments for 1 full arc. The IMRT plans consisted of seven coplanar fields modulated with dynamic-MLC at gantry angles of 0°, 51°, 102°, 204°, 255°, and 306°. Leaf sizes of both MLCs for VMAT and IMRT were 5 mm. The gantry angles of the beams were manually selected based on the morphologic relationships between the PTVs and the OAR.

We employed different optimization algorithms, i.e., the progressive resolution optimizer (PRO) algorithm for the VMAT plans and dose-volume optimizer (DVO) algorithm for the IMRT plans. The PRO algorithm creates the VMAT plans based on dose-volume objectives, and generates a sequence of control points, which define MLC leaf positions and MU/degree as a function of gantry angle. A multi-resolution approach (i.e. simulated annealing method [Otto et al. 2008]) and an objective function (the sum of the dose-volume and user-defined objectives) are used to optimize the VMAT plans. The DVO algorithm determines the optimal field shape and intensity by iteratively conforming the dose distribution to the desired objectives until an optimum solution is reached by using simple gradient optimization.

A four-slice computed tomography (CT) scanner (Mx 8000; Philips, Amsterdam, The Netherlands) was used to acquire planning CT images with dimensions of 512×512 pixels, an in-plane pixel size of 0.977 mm, and a slice thickness of 2.0 mm. Figure 3.1 illustrates the contours of CTV, PTV, rectum, bladder, right femoral head, and left femoral head in an axial view for a low-risk prostate cancer patient. The rectum contours were delineated by inferiorly starting from the anorectal junction and superiorly extending up to the beginning of the

sigmoid at the rectosigmoid junction. The bladder contours were delineated from its base to the dome. The femoral heads contours were delineated to the ball of the femur. The contours of the CTVs, PTVs and OAR were delineated on the planning CT images for each patient based on the consensus between a radiation oncologist (S.O.) and a medical physicist (T.H.) using a commercial radiation treatment planning (RTP) system. The dose distribution images had an in-plane pixel size of 2.5 mm and a slice thickness of 2.0 mm. The voxel size of the original dose distribution data (2.5 mm x 2.5 mm x 2.0 mm) differed from that of the PTV regions on the planning CT images (0.977 mm x 0.977 mm x 2.000 mm). Therefore, nearest-neighbor interpolation and linear interpolation methods were used on the PTV regions and dose distribution data, respectively, so that the isovoxel size (0.977 mm) of the PTV regions was equal to that of the dose distribution data [Parker et al. 1983].

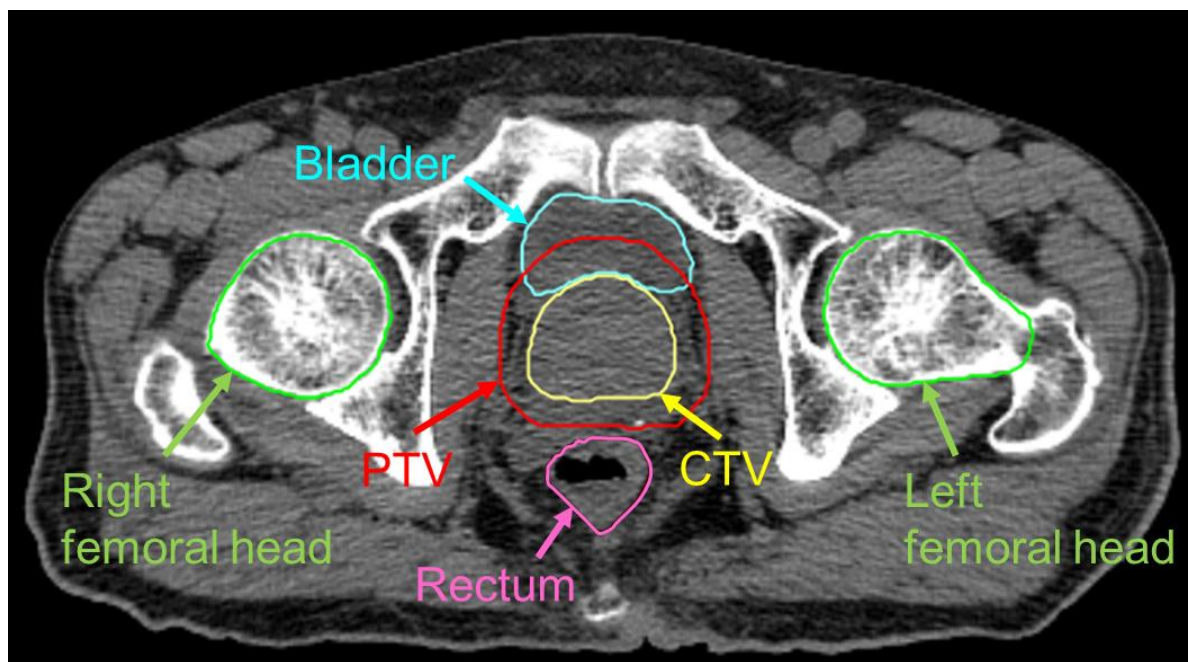


**Fig. 3.1** Illustration of the contours of CTV, PTV, rectum, bladder, right femoral head, and left femoral head in an axial view for a low-risk prostate cancer patient.

### 3.2 Plan evaluation

The following dosimetric indices were evaluated based on the dose-volume histograms of the VMAT and IMRT plans: mean dose, maximum and minimum doses, conformity index (CI), homogeneity index (HI) for PTV and the mean dose and V20 to V70 for OAR including the rectum, bladder, right and left femoral heads, and ROP regions.

The PTV doses were evaluated for the average, minimum, and maximum doses. To quantitatively evaluate dose the conformity and homogeneity in the PTV, the CI and HI were calculated [Hodapp et al. 2012; ICRU 1999; Paddick et al. 2000; Feuvret et al. 2006]. The CI was defined as

$$CI = \frac{TV_{Dp}}{V_{PTV}} \times \frac{TV_{Dp}}{V_{Dp}}, \quad (3.1)$$

where  $TV_{Dp}$  was the PTV covered by the prescribed dose ( $\text{cm}^3$ ),  $V_{PTV}$  was the PTV ( $\text{cm}^3$ ), and  $V_{Dp}$  was the volume of the prescribed dose ( $\text{cm}^3$ ). The HI in the International Commission on Radiation Units and Measurements (ICRU) Report 83 is defined as

$$HI = \frac{D_2 - D_{98}}{D_{50}}, \quad (3.2)$$

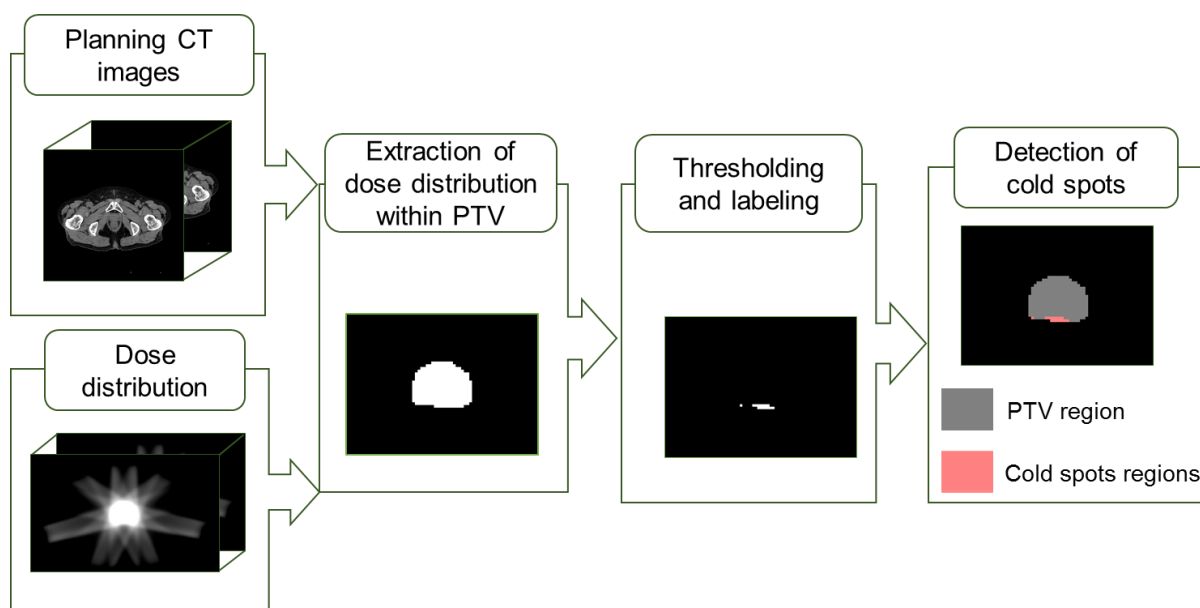
where  $D_2$ ,  $D_{98}$ , and  $D_{50}$  were the minimum dose delivered to 2%, 98%, and 50% of the PTV. An HI value closer to 0 indicates a more homogeneous dose distribution within the PTV. The conformity index is a measure of how well the volume of the prescribed dose conforms to the size and shape of the PTV. A CI value closer to 1 indicates that the volume of the prescribed dose more closely conforms to the PTV.

$V_x$  ( $x = 20, 30, 40, 50, 60, 70$ ) was defined as the percentage of OAR (rectum, bladder, right and left femoral heads, and ROP regions) volume receiving  $x$  Gy and was used to represent the high-dose OAR volume.

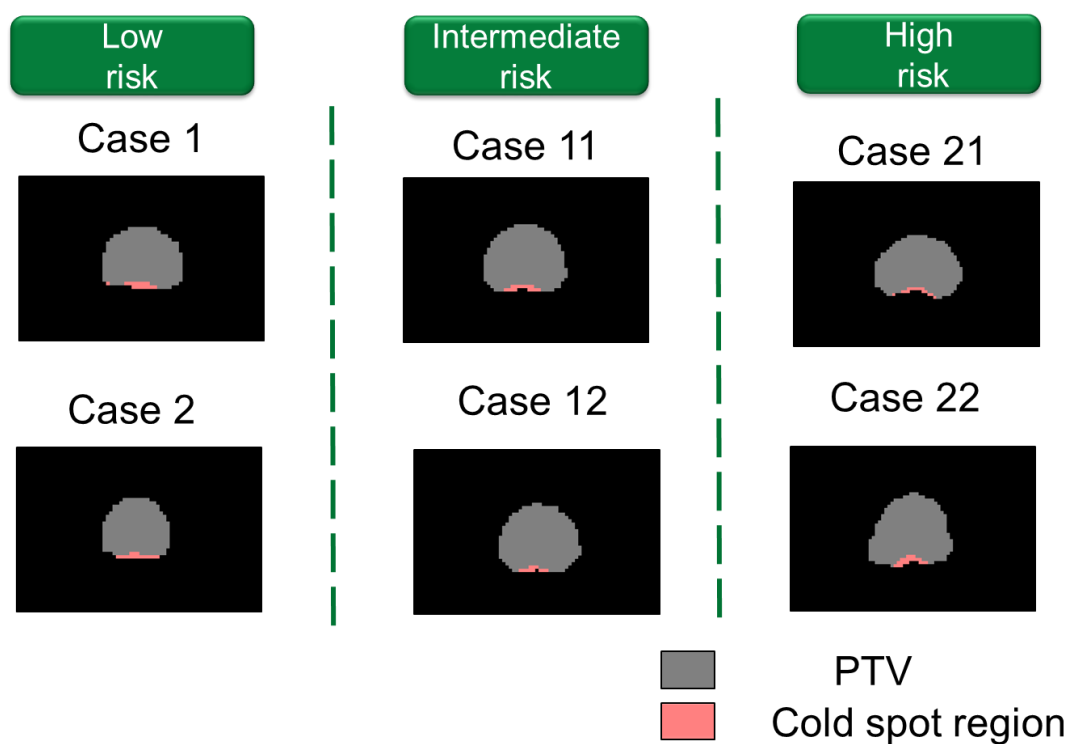
### **3.3 Analysis of cold spots in the dose distributions**

Figure 3.2 shows the overall scheme for the detection of cold spots in dose distributions. First, PTV regions were constructed from contours (DICOM structure data) on planning CT images. Second, the dose distributions within PTVs and ROP regions were extracted from the total dose distributions. Third, cold spot regions were detected by thresholding the dose distributions within PTV regions according to the cold spot definition of dose regions lower than 93% of the prescribed dose. Finally, the detected cold spot regions were labeled using twenty-six connecting labeling [Shapiro et al. 1996; Lumia et al. 1983]. Figure 3.3 shows examples of detected cold spots in planning target volumes of three risk groups for prostate cancer patients. The gray regions indicate PTV and light red regions indicate cold spots. The numbers and volumes of the labeled cold spot regions were then calculated. In addition, for comparison of the VMAT and IMRT plans, the numbers and volumes of the cold spots were normalized by the PTVs. We developed in-house software according to the algorithm described above.





**Fig. 3.2** An overall scheme for the detection of cold spots in dose distributions.



**Fig. 3.3** Examples of detected cold spots in planning target volumes of three risk groups for prostate cancer patients.

### 3.4 3D PD of the probability and distributions of cold spots

Figure 3.4 illustrates an overall scheme developed as in-house software to generate the PD of the probability and distributions of cold spots. The PD of the probability and distributions of cold spots were constructed by registration of all PTV and detected cold spots to a reference PTV (a median PTV) using a centroid matching technique [Shibayama et al. 2017]. The PD ( $P(\mathbf{x}_i)$ ) of the probability and distributions of cold spots was calculated as

$$P(\mathbf{x}_i) = \frac{1}{N} \sum_{n=1}^N f_n(\mathbf{x}_i), \quad (3.3)$$

where  $\mathbf{x}_i$  was the 3D coordinate of  $i$ -th voxel,  $n$  was the case number,  $N$  was the number of cases, and  $f_n(\mathbf{x}_i)$  was the  $i$ -th voxel value (one or zero) of cold spots regions for a  $n$ -th case.

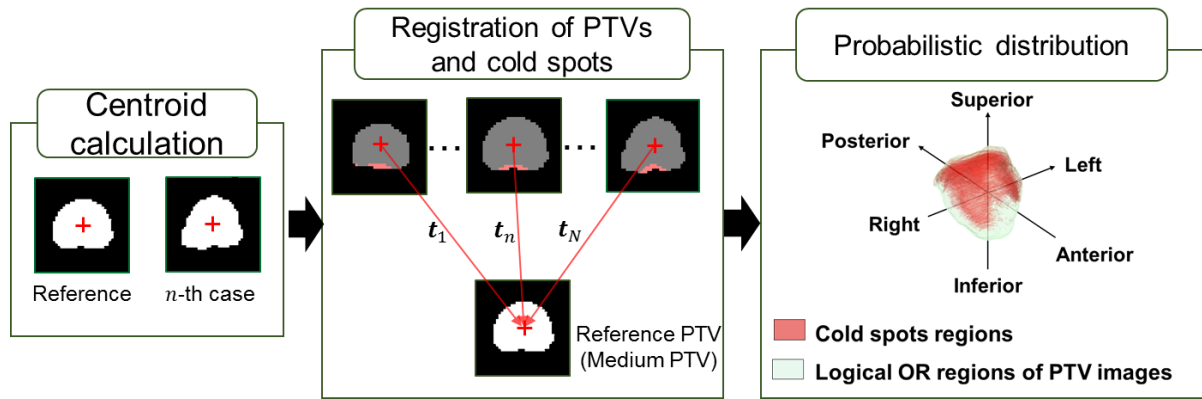


**Fig. 3.4** An overall scheme for generating a probabilistic distribution of the probability and distributions of cold spots

Furthermore, we investigated the volumes of the cold-spot-existence PD by changing the probabilities. For 3D visualizations and analyses of the PD of the probability and distributions of cold spots, a red color with an opacity, which represented the degree of color transparency, was set to the value of the probability of the existence of cold spots ranging from 0 to 1. A logical OR indicates the mathematical operation in logic or the logical disjunction. The logical OR region of the PTVs is a set of voxels, in which the logical ORs

are one after registering all PTVs to the reference PTV. Each PTV consists of a one-value voxel, but the outside voxels include a zero-value voxel. The logical OR region of the PTV was also visualized as a green color in order to analyze the location of cold spots in the PTV.

The visualization tool presented in this study can be used for verification of the presence or absence of cold spot regions in the CTV, because cold spots should not be located within the CTV but should be at the periphery of the PTV [Mundt et al. 2005] according to RTOG H-0222.

### **3.5 Statistical analysis**

To evaluate the differences between the VMAT and IMRT plans, statistical analysis was performed using two-sided paired Student's *t*-tests. The difference was considered statistically significant for P-values less than 0.05.

### **3.6 Results**

Tables 2 – 5 show the averages and standard deviations of the dosimetric indices for the PTV, rectum, bladder, ROP, right femoral head, and left femoral head of the VMAT and IMRT plans for the low-risk group, the intermediate-risk group, the high-risk group, and all risk groups, respectively. As for the PTV, there were no statistical significant differences in the CI and HI between VMAT and IMRT plans among the three risk groups (Tables 2 – 4). However, VMAT had statistically better dose conformity than that of the IMRT plans, whereas VMAT had statistically worse dose homogeneity than that of the IMRT plans for all risk groups (Table 5).

For the rectum, the VMAT plans resulted in a lower average mean dose to the rectum and lower volume percentages of the rectum at every dose (20, 30, 40, 50, and 60 Gy) than those of the IMRT plans (Table 5). All differences between the VMAT and IMRT plans were statistically significant. These results indicate that the VMAT provided a dosimetric advantage by sparing the dose to the rectum compared to the IMRT plans. The bladder

received a greater average mean dose in the VMAT compared to that in the IMRT plans (Table 5). However, the difference between the plans was not statistically significant. The VMAT resulted in statistically lower volume percentages received by the bladder at 50, 60, and 70 Gy than those of the IMRT plans (Table 5). Therefore, VMAT could reduce higher dose volumes for the bladder, compared with IMRT.

For the ROP region, the average mean dose was lower in the VMAT compared with the IMRT plans, and the difference was not statistically significant (Table 5). The V40 of the ROP region was 100% for both VMAT and IMRT plans (Table 5). For the femoral head, compared with the IMRT plans, average mean doses to femoral heads were greater in the VMAT plans for both the right and left femoral heads (Table 5). The V40 of the right and left femoral heads was 0% for both the VMAT and IMRT plans (Table 5). These results indicated that IMRT produced better dose sparing of the femoral heads than VMAT.

**Table 2.** Averages and standard deviations of the dosimetric indices for PTV, rectum, bladder, ROP, right femoral head, and left femoral head of VMAT and IMRT plans for the low-risk group.

		VMAT		IMRT		
		Average	±SD	Average	±SD	P value
PTV						
	Mean dose (Gy)	76.00	0.00	76.00	0.00	-
	Maximum dose(Gy)	79.51	0.65	78.13	0.36	<0.001
	Minimum dose (Gy)	61.37	2.37	62.19	2.36	0.111
	CI	0.964	0.013	0.958	0.014	0.118
	HI	0.103	0.022	0.096	0.021	0.344
Rectum						
	Mean dose (Gy)	26.82	2.78	28.41	2.48	<0.001
	V20 (%)	53.71	4.28	58.81	5.17	0.005
	V30 (%)	34.89	6.19	38.81	4.06	0.007
	V40 (%)	23.35	5.60	25.46	4.92	0.003

V50 (%)	15.79	3.97	17.41	4.00	<b>&lt;0.001</b>
V60 (%)	10.03	2.59	11.16	2.62	<b>&lt;0.001</b>
V70 (%)	3.80	1.25	3.71	1.25	0.612
Bladder					
Mean dose (Gy)	26.29	11.61	27.29	11.59	<b>0.008</b>
V20 (%)	46.96	23.07	49.34	23.09	<b>0.004</b>
V30 (%)	38.04	21.54	40.26	21.58	<b>0.004</b>
V40 (%)	28.91	16.98	30.15	16.91	<b>0.017</b>
V50 (%)	21.67	12.27	22.76	12.53	<b>0.015</b>
V60 (%)	16.23	8.86	16.71	12.53	0.207
V70 (%)	10.15	5.96	10.76	5.52	<b>0.012</b>
ROP					
Mean dose (Gy)	69.89	1.01	69.92	1.19	0.890
V40 (%)	100.00	0.00	100.00	0.00	-
Right femoral head					
Mean dose (Gy)	15.35	2.96	14.03	2.73	0.217
V40 (%)	0.00	0.00	0.00	0.00	-
Left femoral head					
Mean dose (Gy)	16.12	1.55	13.89	2.73	<b>0.020</b>
V40 (%)	0.00	0.00	0.00	0.00	-

PTV: planning target volume; ROP: rectum overlapped with PTV; VMAT: volumetric modulated arc therapy; IMRT: intensity modulated radiation therapy; SD: standard deviation; CI: conformity index; HI: homogeneity index; Vx: percentage volume receiving at least x Gy. Values in bold are statistically significant.

**Table 3.** Averages and standard deviations of the dosimetric indices for PTV, rectum, bladder, ROP, right femoral head, and left femoral head of VMAT and IMRT plans for the intermediate-risk group.

		VMAT		IMRT		
		Average	±SD	Average	±SD	P value
PTV						
	Mean dose (Gy)	76.00	0.00	76.00	0.00	-

Maximum dose(Gy)	79.40	0.47	78.32	0.60	<b>0.001</b>
Minimum dose (Gy)	60.27	2.73	62.92	2.22	<b>0.037</b>
CI	0.966	0.012	0.965	0.013	0.937
HI	0.089	0.016	0.083	0.016	0.154
Rectum					
Mean dose (Gy)	28.90	1.89	31.40	2.12	<b>0.001</b>
V20 (%)	61.38	6.96	69.17	6.40	<b>&lt;0.001</b>
V30 (%)	38.77	6.72	45.75	10.00	<b>0.020</b>
V40 (%)	24.44	3.49	28.91	3.90	<b>0.003</b>
V50 (%)	16.40	2.43	18.96	2.46	<b>&lt;0.001</b>
V60 (%)	10.33	1.58	12.13	1.66	<b>&lt;0.001</b>
V70 (%)	4.12	0.68	4.47	0.75	<b>0.015</b>
Bladder					
Mean dose (Gy)	26.36	9.61	26.90	9.69	0.216
V20 (%)	46.55	18.84	47.93	18.48	0.162
V30 (%)	37.65	16.55	39.06	16.48	0.054
V40 (%)	28.70	12.98	29.52	12.85	0.135
V50 (%)	21.51	9.90	22.61	10.34	<b>0.011</b>
V60 (%)	16.10	7.57	16.99	8.20	<b>0.016</b>
V70 (%)	10.06	5.32	11.39	5.94	<b>0.003</b>
ROP					
Mean dose (Gy)	70.62	0.95	70.79	0.73	0.237
V40 (%)	100.00	0.00	100.00	0.00	-
Right femoral head					
Mean dose (Gy)	14.14	4.65	13.03	4.82	0.148
V40 (%)	0.00	0.00	0.00	0.00	-
Left femoral head					
Mean dose (Gy)	15.33	5.16	13.73	4.89	<b>0.038</b>
V40 (%)	0.00	0.00	0.00	0.00	-

PTV: planning target volume; ROP: rectum overlapped with PTV; VMAT: volumetric modulated arc therapy; IMRT: intensity modulated radiation therapy; SD: standard deviation; CI: conformity index; HI: homogeneity index; Vx: percentage volume receiving at least x Gy.

Values in bold are statistically significant.

**Table 4.** Averages and standard deviations of the dosimetric indices for PTV, rectum, bladder, ROP, right femoral head, and left femoral head of VMAT and IMRT plans for the high-risk group.

		VMAT		IMRT		P value
		Average	±SD	Average	±SD	
PTV						
	Mean dose (Gy)	76.00	0.00	76.00	0.00	-
	Maximum dose(Gy)	79.20	0.48	78.35	0.80	<b>&lt;0.001</b>
	Minimum dose (Gy)	62.11	1.89	62.87	2.73	0.329
	CI	0.959	0.017	0.967	0.015	0.187
	HI	0.091	0.019	0.081	0.018	0.050
Rectum						
	Mean dose (Gy)	27.63	3.26	29.91	3.51	<b>&lt;0.001</b>
	V20 (%)	57.29	9.63	62.62	9.88	<b>0.007</b>
	V30 (%)	36.73	8.09	42.63	7.82	<b>&lt;0.001</b>
	V40 (%)	24.26	4.59	28.45	5.09	<b>&lt;0.001</b>
	V50 (%)	16.53	2.98	20.65	4.98	<b>0.002</b>
	V60 (%)	10.45	1.95	14.47	6.13	<b>0.039</b>
	V70 (%)	4.19	1.02	6.64	5.67	0.174
Bladder						
	Mean dose (Gy)	27.24	9.97	25.55	10.24	0.261
	V20 (%)	48.90	19.80	46.08	19.45	0.343
	V30 (%)	38.19	19.84	36.05	18.86	0.445
	V40 (%)	28.65	16.36	27.05	15.63	0.429
	V50 (%)	20.21	11.47	20.96	12.46	0.860
	V60 (%)	15.55	8.08	15.64	9.09	0.929
	V70 (%)	10.02	5.23	10.43	5.94	<b>0.009</b>
ROP						
	Mean dose (Gy)	70.44	0.62	70.92	1.27	0.219
	V40 (%)	100.00	0.00	100.00	0.00	
Right femoral head						
	Mean dose (Gy)	12.57	4.44	12.00	4.52	0.418
	V40 (%)	0.00	0.00	0.00	0.00	

Left femoral head

Mean dose (Gy)	14.03	5.24	12.46	12.46	0.014
V40 (%)	0.00	0.00	0.00	0.00	

PTV: planning target volume; ROP: rectum overlapped with PTV; VMAT: volumetric modulated arc therapy; IMRT: intensity modulated radiation therapy; SD: standard deviation; CI: conformity index; HI: homogeneity index; Vx: percentage volume receiving at least x Gy. Values in bold are statistically significant.

**Table 5.** Averages and standard deviations of the dosimetric indices for PTV, rectum, bladder, ROP, right femoral head, and left femoral head of VMAT and IMRT plans for all risk groups.

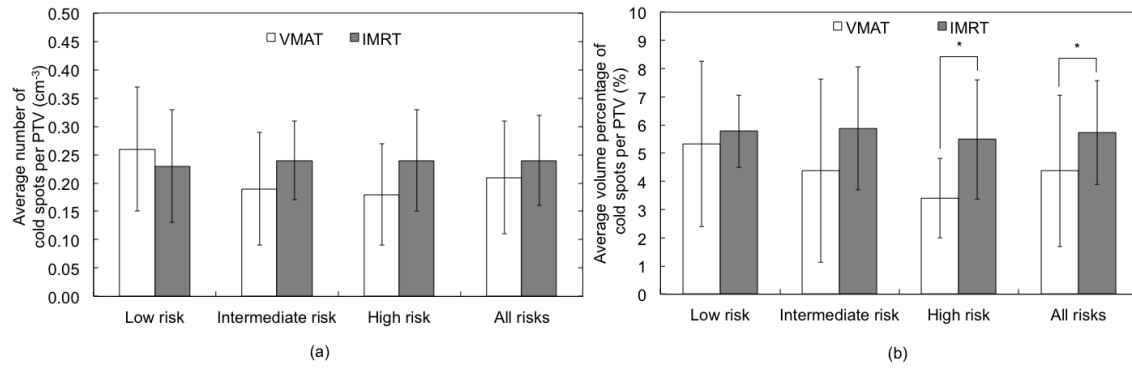
		VMAT		IMRT		P value
		Average	±SD	Average	±SD	
PTV						
	Mean dose (Gy)	76.00	0.00	76.00	0.00	-
	Maximum dose(Gy)	79.36	0.53	78.28	0.61	<b>&lt;0.001</b>
	Minimum dose (Gy)	61.28	2.38	62.68	2.39	<b>0.007</b>
	CI	0.963	0.014	0.954	0.014	<b>0.046</b>
	HI	0.094	0.019	0.086	0.019	<b>0.010</b>
Rectum						
	Mean dose (Gy)	27.81	2.75	29.96	2.96	<b>&lt;0.001</b>
	V20 (%)	57.59	7.85	63.67	8.47	<b>&lt;0.001</b>
	V30 (%)	36.86	7.02	42.54	8.01	<b>&lt;0.001</b>
	V40 (%)	24.05	4.44	27.72	4.73	<b>&lt;0.001</b>
	V50 (%)	16.27	3.04	19.12	4.07	<b>&lt;0.001</b>
	V60 (%)	10.29	1.98	12.71	4.22	<b>&lt;0.001</b>
	V70 (%)	4.05	0.97	4.95	3.66	0.130
Bladder						
	Mean dose (Gy)	26.67	9.97	26.52	10.10	0.511
	V20 (%)	47.14	19.73	47.66	18.32	<b>0.017</b>
	V30 (%)	37.97	18.59	38.30	18.32	0.701
	V40 (%)	37.97	18.59	28.74	14.90	0.126
	V50 (%)	21.44	11.39	22.04	11.39	<b>0.019</b>



V60 (%)	15.94	8.45	16.41	8.45	<b>0.001</b>
V70 (%)	10.09	5.61	10.85	5.61	<b>&lt;0.001</b>
ROP					
Mean dose (Gy)	70.34	0.88	70.58	1.14	0.115
V40 (%)	100.00	0.00	100.00	0.00	-
Right femoral head					
Mean dose (Gy)	13.70	4.20	12.79	4.18	<b>0.038</b>
V40 (%)	0.00	0.00	0.00	0.00	-
Left femoral head					
Mean dose (Gy)	14.92	4.20	13.19	4.33	<b>&lt;0.001</b>
V40 (%)	0.00	0.00	0.00	0.00	-

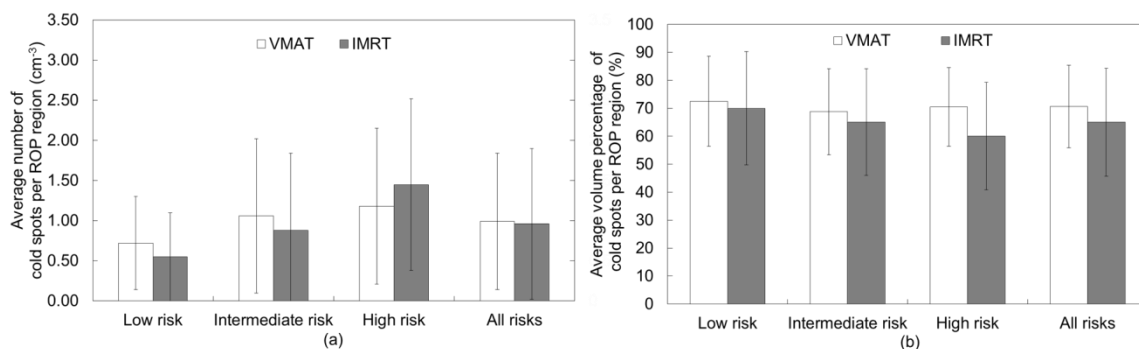
PTV: planning target volume; ROP: rectum overlapped with PTV; VMAT: volumetric modulated arc therapy; IMRT: intensity modulated radiation therapy; SD: standard deviation; CI: conformity index; HI: homogeneity index; Vx: percentage volume receiving at least x Gy. Values in bold are statistically significant.

Figure 3.5(a) shows the average numbers of cold spots per PTV of the three risk groups for the VMAT and IMRT plans. The error bars indicate the standard deviations. The averages  $\pm$  standard deviations of the numbers of cold spots per PTV of all risk groups for the VMAT and IMRT plans were  $0.21 \pm 0.10 \text{ cm}^{-3}$  and  $0.24 \pm 0.08 \text{ cm}^{-3}$ , respectively ( $P = 0.158$ ). There was no significant difference between the VMAT and IMRT plans for the average numbers of cold spots per PTV for each type of risk. Figure 3.5(b) shows the average volume percentages of cold spots in the PTV of the three risk groups in the VMAT and IMRT plans. The average volume percentage of cold spots per PTV for all risks was  $4.37 \pm 2.68\%$  for the VMAT, which was smaller than the  $5.72 \pm 1.84\%$  observed for the IMRT plans ( $P = 0.007$ ). As for the high-risk group, the average volume percentage of cold spots for VMAT was statistically smaller than that for IMRT plans ( $P < 0.001$ ).



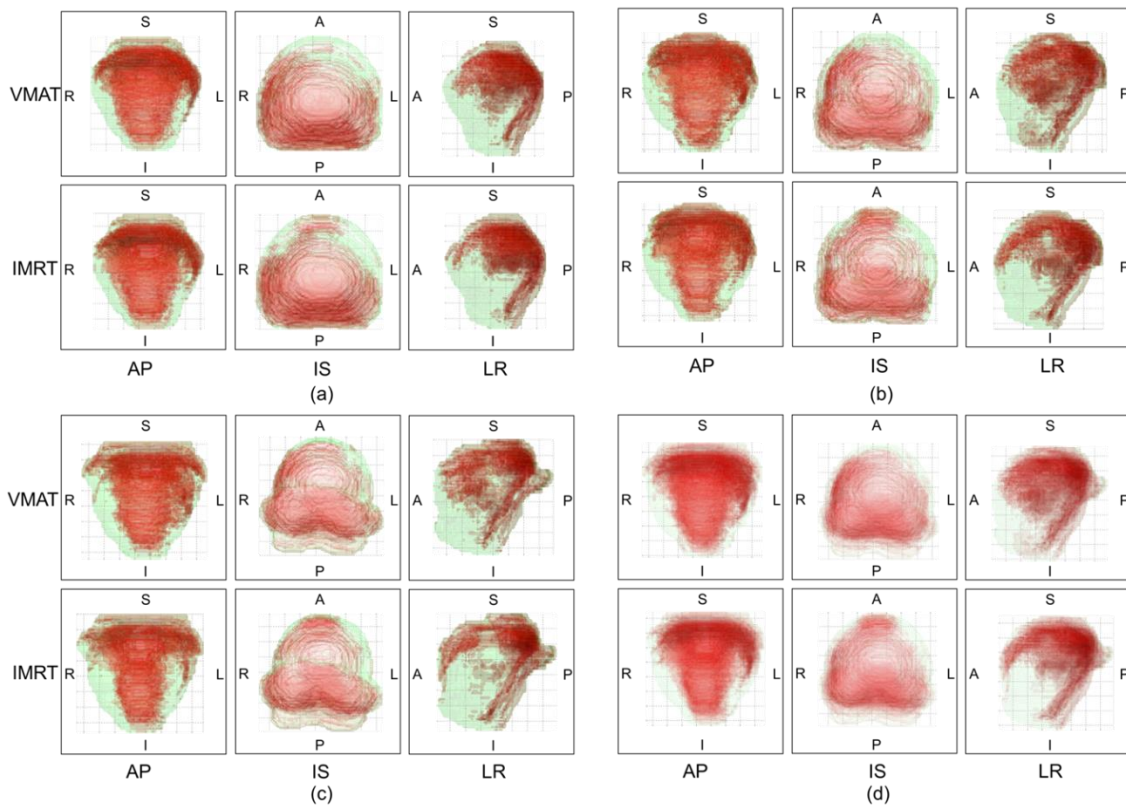
**Fig. 3.5 (a)** Average numbers and **(b)** volume percentages of cold spots per PTV of 3 risk groups for VMAT and IMRT plans. The error bars and asterisks indicate the standard deviations and statistical significances ( $P < 0.05$ ), respectively.

Figures 3.6(a) and 3.6(b) show the average numbers and volume percentages of cold spots per ROP region of the three risk groups for the VMAT and IMRT plans, respectively. The average of cold spots per ROP region of all risk groups for VMAT number ( $0.99 \pm 0.85 \text{ cm}^{-3}$ ) did not significantly differ from that ( $0.96 \pm 0.94 \text{ cm}^{-3}$ ) for IMRT plans ( $P = 0.827$ ), as shown in Figure 3.6(a). Additionally, the average volume percentage ( $70.61 \pm 14.77\%$ ) of cold spots per ROP region for the VMAT did not significantly differ from that ( $65.07 \pm 19.3\%$ ) for the IMRT plans ( $P = 0.087$ ), as shown in Figure 3.6(b). There was no significant difference between the VMAT and IMRT plans regarding the average number and volume percentage of cold spots per ROP region for each type of risk.



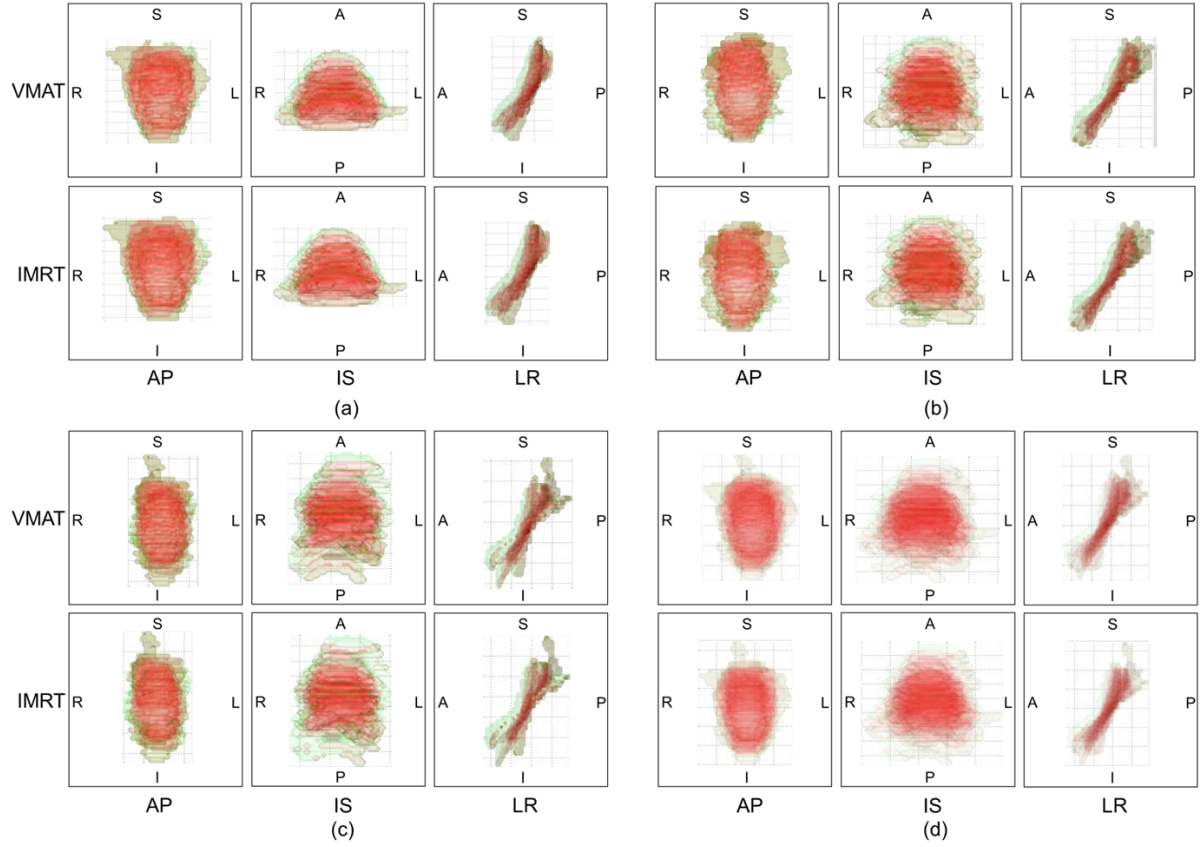
**Fig. 3.6 (a)** Average numbers and **(b)** volume percentages of cold spots per ROP region of 3 risk groups for VMAT and IMRT plans. The error bars indicate the standard deviations.

Figure 3.7 shows the 3D PDs of the probability and distributions of cold spots in the VMAT and IMRT plans for the low-risk group, the intermediate-risk group, the high-risk group, and all risk groups. The logical OR region of the PTVs is shown in light green, while the PD of the probability and distributions of cold spots is shown in red with opacity. Figures 3.7(a) – (d) show that the cold spots are widely distributed throughout PTVs in both VMAT and IMRT plans. However, in the anterior-posterior (AP) and left-right (LR) views, most of the cold spots are distributed on the posterior and upper PTVs for both plans. In addition, the 3D PDs of the probability and distributions of cold spots in the ROP regions in the VMAT and IMRT plans for low-risk group, intermediate-risk group, high-risk group, and all-risk groups are shown in Figures 3.8(a) – (d).



**Fig. 3.7** Three-dimensional probabilistic distributions of the probability and distributions of cold spots in VMAT and IMRT plans in anterior-posterior (AP), inferior-superior (IS), and left-right (LR) views for **(a)** low-risk group, **(b)** intermediate-risk group, **(c)** high-risk group, and **(d)** all-risk groups.

Table 6 shows volumes of cold-spot-existence-probability distributions more than several probabilities for VMAT and IMRT plans. The probabilistic volumes of cold spots were estimated at different distribution probabilities of cold spots for VMAT and IMRT plans. The volume ( $3.86 \text{ cm}^3$ ) more than a distribution probability of 0.3 of cold spots for VMAT was smaller than that ( $5.10 \text{ cm}^3$ ) for IMRT plans. These probabilistic volumes of cold spots indicate that the probability of the existence of cold spots in VMAT is smaller than IMRT plans. However, at low probabilities of cold spots (0.1), the volume of cold spots for VMAT ( $239.08 \text{ cm}^3$ ) was larger than that for IMRT plans ( $235.91 \text{ cm}^3$ ). This is because the cold spots in VMAT are more widely distributed than those of IMRT plans, as shown in Figures 3.7(a) – (d).



**Fig. 3.8** Three-dimensional probabilistic distributions of the probability and distributions of cold spots in ROP regions in VMAT and IMRT plans in anterior-posterior (AP), inferior-superior (IS), and left-right (LR) views for **(a)** low-risk group, **(b)** intermediate-risk group, **(c)** high-risk group, and **(d)** all-risk groups.

**Table 6.** Volumes of cold-spot-existence-probability distributions for several probabilities in VMAT and IMRT plans.

Probability for threshold	Probabilistic volume of cold spots (cm <sup>3</sup> )	
	VMAT	IMRT
0	1019.24	1019.14
0.1	239.08	235.91
0.2	44.35	44.51
0.3	3.86	5.10
0.4	0.03	0.11

VMAT: volumetric modulated arc therapy; IMRT: intensity modulated radiation therapy.

### 3.7 Discussion

This study compared the dosimetric qualities of VMAT and IMRT plans using dosimetric indices and analyzed cold spots in prostate cancer. The VMAT provided dosimetric advantages over the IMRT plans with respect to target dose conformity, dose sparing of the rectum and bladder (Table 5), and cold spots (Figure 3.5(b), Table 6), but achieved worse target dose homogeneity and dose sparing of the right and left femoral heads compared to those of the IMRT plans (Table 5).

Previous studies have reported similar results for target dose conformity and OAR dose-sparing in dosimetric comparisons for the treatment of prostate cancer [Palma et al. 2008; Wolff et al. 2009; Quan et al. 2012; Guckenberger et al. 2009; Kjaer-Kristoffersen et al. 2009; Ost et al. 2011; Shaffer et al. 2009]. However, some dosimetric comparison results in the present study differed from those reported other studies [Yoo et al. 2009; Sze et al. 2012; Kopp et al. 2011]. Yoo et al. showed a better dose conformity in the PTV but worse rectum and bladder dose-sparing by VMAT compared to those in IMRT plans [Yoo et al. 2009]. Differences in VMAT and IMRT techniques, plan objectives, beam angles, etc., may have contributed to this difference in results. Another factor may be related to differences in the volume and shape of the PTV due to different CTV definitions at different institutes and differences in patient risk groups. All of these factors might affect the dosimetric outcomes.

Divergent delineation policies for the three risk groups in prostate cancer cases may lead to differences in the results of VMAT and IMRT plans. There were some differences in the results among risk groups, for example, results for PTV and femoral head in Table 5 (summary of all risk groups) were partially different from those in Tables 2 (low-risk group), 3 (intermediate-risk group), 4 (high-risk group). For instance, there were no statistically significant differences in average minimum doses to PTV between VMAT and IMRT plans

in low- and high-risk groups (Tables 2 and 4), whereas average minimum doses in VMAT plans were significantly lower than those in IMRT plans, with respect to intermediate-risk and all risk groups (Tables 3 and 5). In addition, there were no statistically significant differences in the CI and HI among VMAT and IMRT plans between the 3 risk groups (Tables 2 - 4); however, there were statistically significant differences in those parameters when all risk groups were analyzed together (Table 5). Furthermore, the delineation policy of three risk groups in prostate cancer cases could have an impact on the results pertaining to the femoral head. In the intermediate-risk and all risk groups (Tables 3 and 5) the average mean doses to left femoral heads in VMAT plans were significantly greater than those in IMRT plans. Additionally, only analyzing all risk groups together (Table 5) showed that the mean dose to the right femoral heads was significantly greater in VMAT compared with IMRT plans.

The difference of optimization algorithms between VMAT (PRO algorithm) and IMRT (DVO algorithm) may affect the dosimetric results of VMAT and IMRT plans. While a simple gradient method was employed for the IMRT plans, a simulated annealing method was employed for the VMAT plans. In the latter, one of the variables in the simulated annealing is randomly selected and its value is randomly increased or decreased by a small amount [Taqaddas 2011]. This could result in better optimization results and may achieve better plans, because trapping in the local minimum is avoided [Khan 2007]. For example, the effect of difference in optimization algorithms was shown in Figure 3.5(b) for the high-risk group. In addition, we think that VMAT could reduce cold spot occurrence by irradiation from many gantry angles and delivery times optimized in that algorithm.

Because cold spots in the PTV could induce tumor recurrence, we also analyzed the numbers, volumes, and distributions of cold spots between the VMAT and IMRT plans. Figures 3.5(a) and 3.5(b) indicate that VMAT plans result in cold spots with smaller volumes

in the PTV than those in the IMRT plans, as shown by the probability of 0.3 of cold spots in Table 6, whereas the cold spots in the VMAT were distributed more widely than those in the IMRT plans, as shown in Figures 3.7(a) – (d). The reason for this phenomenon is that the VMAT can irradiate from more directions than IMRT, which averages the VMAT irradiation to a rotating target, whereas IMRT irradiates from only seven directions. Figures 3.7(a) – (d) show the distributions of cold spots on the posterior and upper PTVs for all types of risk groups in the VMAT and IMRT plans. The reason for this distribution is that the ROP region is not regarded as a target for dose calculation in planning the radiotherapy of prostate cancer in order to avoid high irradiating doses to the rectum (OAR) [McLaughlin et al. 1999; Serrano et al. 2017]. Therefore, cold spots were distributed throughout nearly all of parts of the ROP regions (Figures 3.8(a) – (d)), as also evidenced by the volume percentages of cold spots per ROP for the VMAT and IMRT plans in Figure 3.6(b). Considering the differences in the distributions of cold spots between the VMAT and IMRT plans, the volumes of cold spots in the VMAT was smaller than those of the IMRT (Figure 3.5(b)), whereas there was no significant difference in the volume of cold spots in the ROP regions between the plans (Figure 3.6(b)). These results indicated that the volume of cold spots in other parts of the PTV (except for the ROP regions) in VMAT was smaller than that of the IMRT plans.

To understand how much the cold spot occurrence affects DVH, we investigated the relationship between the volume percentage of cold spots per PTV (%) and  $D_{99}$  (Gy) for (a) VMAT and (b) IMRT plans, as shown in Figure 3.9. Figure 3.9 indicated that  $D_{99}$  representing the minimum dose delivered to 99% of the PTV decreased with increasing of the volume of cold spots for both VMAT and IMRT plans. The average  $\pm$  SD of  $D_{99}$  for VMAT plans was  $68.68 \pm 2.63$  Gy, which was smaller than  $69.42 \pm 1.73$  Gy for IMRT plans ( $P = 0.002$ ). In other words, there are negative correlations between the cold spot volume per PTV and  $D_{99}$  for VMAT and IMRT plans. This result does not correspond that the average



volume percentage of cold spots per PTV for the VMAT plans was  $4.37 \pm 2.68\%$ , which was smaller than the  $5.72 \pm 1.84\%$  observed for IMRT plans ( $P = 0.007$ ). Consequently, the cold spots would not affect the DVH at least  $D_{99}$ .

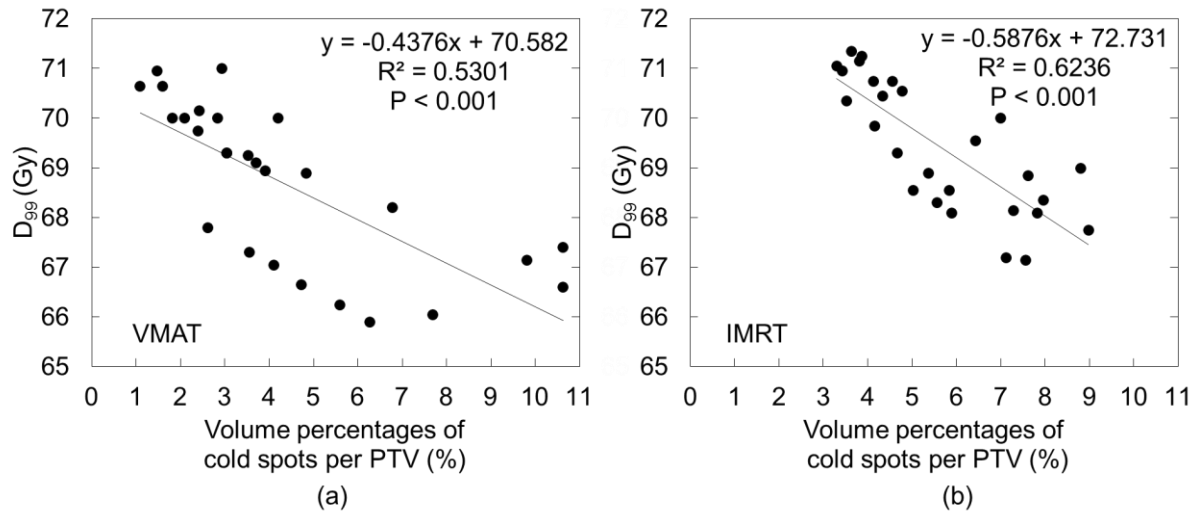


**Fig. 3.9** Relationship between volume percentages of cold spots per PTV and  $D_{99}$  for (a) VMAT and (b) IMRT plans.

This study had three limitations. First, we used definition of the cold spots based on the use of the trial guidelines of the RTOG H-0222 in head and neck cancers. Second, many cold spots were distributed on the upper PTVs, as shown in Figures 3.7(a) – (d). Further consideration is needed to assess the distributions of these cold spots in VMAT and IMRT plans. Third, 30 patients with only 10 cases for each risk group were selected for this study. Therefore, data from a larger number of cancer patients in each risk group are required in order to improve the accuracy of the prediction of the PD of cold spots.

## **Chapter 4 Conclusions**

In this thesis, we compared the dosimetric indices, i.e. the mean, maximum, and minimum doses and conformity and homogeneity indexes were evaluated for the PTV; the mean dose and V20 to V70 for OAR including the rectum, bladder, right and left femoral heads, and ROP regions, and analyzed the numbers, volume percentages, and probabilistic distributions of the probability and distributions of cold spots for VMAT and IMRT prostate cancer plans.

In Chapter 1, we introduced the potential of analysis (magnitude and volume) and visualization of cold spots of the PTV and ROP region and the potential of comparison of VMAT and IMRT plans accounting for cold spots.

In Chapter 2, we introduced the basic theory of inverse treatment planning and optimization in IMRT and VMAT.

In Chapter 3, we compared VMAT with IMRT in prostate cancer plans accounting for cold spots in 3 risk groups. We proposed an analysis and visualization of cold spots in the PTV and ROP regions for prostate cancer radiation therapy. Additionally, we evaluated the results by using a statistical analysis and visualization to compare dosimetric indices and number, volume of cold spots of the VMAT and IMRT plans. We concluded that VMAT plans achieved better target dose conformity, OAR (rectum, bladder) dose-sparing, and smaller cold spots than those of the IMRT plans in the radiation treatment of prostate cancer.

## Acknowledgements

I would like to express my deepest appreciation to my supervisor, Prof. Hidetaka Arimura, for his time, patience, and precious advices and comments about my research. Beside the invaluable scientific supervision, his personal opinions and advices helped me grow up and will have everlasting impact on my whole life. I also express my gratitude to his wife, Mrs. Chikako Arimura, who has been always kind and helpful during my tough time in Japan.

I would like to deeply thank all Department of Clinical Radiology staff members in Kyushu University Hospital, especially Mr. Taka-aki Hirose who kindly collaborated with us in the experimental part of this research. I'm so grateful to all faculty members of Division of Medical Quantum Science, Department of Health Sciences, Faculty of Medical Sciences in Kyushu University and all Arimura Laboratory members who provided me with the precious comments and advices, especially Mr. Ryosuke Asamura, whose great support and contribution made this research possible and my tutor Ms. Ayumi Nonaka, whose great kindness and support made my daily life easier in Japan.

My very special gratitude is for the one who has been always brought happiness, support, encouragement, and care for me, listened, swallowed my tears, and eased my pain in the most difficult time, Mr. Kohmura Hiroaki. Never let you go.

Last but not least, the forever gratitude goes to the ones who brought me to life and have always believed in me: my father Tran Dinh Tam and mother Nguyen Thi Thanh Tram, besides my brother Hoai Nam and sisters Yen Phuong, Phuong Thao, Minh Chau. They have always been provided me big love, care and support. I love them more than I ever found a way to say to them.

I'm honoured for receiving MEXT scholarship, Sato Yo International Foundation, and a Fellowship (DC1) from the Japanese Society for Promotion of Science (JSPS), by which I could live in Japan and pursue my PhD degree course.

## References

- Ferlay J, Soerjomataram I, Dikshit R, et al. Cancer incidence and mortality worldwide: Sources, methods and major patterns in GLOBOCAN 2012. *Int J Cancer*. 2015;136:359-386.
- Kitazawa T, Matsumoto K, Fujita S, et al. Cost of illness of the prostate cancer in Japan - a time-trend analysis and future projections. *BMC Health Serv Res*. 2015;15:453.
- Ogawa K, Nakamura K, Sasaki T, et al. Radical external beam radiotherapy for clinically localized prostate cancer in Japan: changing trends in the patterns of care process survey. *Int J Radiat Oncol Biol Phys*. 2011;81:1310-8.
- King CR, Dipetrillo TA, Wazer DE, et al. Optimal radiotherapy for prostate cancer: predictions for conventional external beam, IMRT, and brachytherapy from radiobiologic models. *Int J Radiat Oncol Biol Phys*. 2000;46:165-72.
- Ezzell GA, Galvin JM, Low D, et al. Guidance document on delivery, treatment planning, and clinical implementation of IMRT: Report of the IMRT Subcommittee of the AAPM Radiation Therapy Committee. *Med Phys*. 2003;30:2089-2115.
- Hodapp N. The ICRU Report 83: prescribing, recording and reporting photon-beam intensity-modulated radiation therapy (IMRT). *Strahlenther Onkol*. 2012;188:97–99.
- Rana S. Intensity modulated radiation therapy versus volumetric intensity modulated arc therapy. *Journal of Medical Radiation Sciences*. 2013;60:81-83.
- Otto K. Volumetric modulated arc therapy: IMRT in a single gantry arc. *Med Phys*. 2008;35:310–317.
- Jeraj R, Keall PJ, Siebers JV. The effect of dose calculation accuracy on inverse treatment planning. *Phys Med Biol*. 2002;47:391–407.
- Mundt AJ, Roeske JC. Intensity Modulated Radiation Therapy: A Clinical Perspective. BC Decker Inc., Hamilton, Ontario, 2005.
- Dogan N, Siebers JV, Keall PJ, et al. Improving IMRT dose accuracy via deliverable Monte Carlo optimization for the treatment of head and neck cancer patients. *Med Phys*. 2006;33:4033–4043.

- Bortfeld T, Craft D, Dempsey JF, et al. Evaluating target cold spots by the use of tail EUDs. *Int J Radiat Oncol Biol Phys.* 2008;71:880-889.
- Tomé WA, Fowler JF. On cold spots in tumor subvolumes. *Med Phys.* 2002;29:1590-8
- Vora SA, Wong WW, Schild SE et al. Outcome and toxicity for patients treated with intensity modulated radiation therapy for localized prostate cancer. *J Urol.* 2013;190:521-6.
- Zaorsky NG, Shaikh T, Murphy CT, et al. Comparison of outcomes and toxicities among radiation therapy treatment options for prostate cancer. *Cancer Treat Rev.* 2016;48:50-60.
- Palma D, Vollans E, James K, et al. Volumetric modulated arc therapy for delivery of prostate radiotherapy: comparison with intensity-modulated radiotherapy and three-dimensional conformal radiotherapy. *Int J Radiat Oncol Biol Phys.* 2008;72:993-1001.
- Wolff D, Stieler F, Welzel G, et al. Volumetric modulated arc therapy (VMAT) vs. serial tomotherapy, step-and-shoot IMRT and 3D-conformal RT for treatment of prostate cancer. *Radiother Oncol.* 2009;93:226-233.
- Quan EM, Li X, Li Y, et al. A Comprehensive Comparison of IMRT and VMAT Plan Quality for Prostate Cancer Treatment. *Int J Radiat Oncol Biol Phys* 2012;83:1169-1178.
- Guckenberger M, Richter A, Krieger T, et al. Is a single arc sufficient in volumetric-modulated arc therapy (VMAT) for complex-shaped target volumes?. *Radiother Onco.* 2009;93:259–65.
- Kjaer-Kristoffersen F, Ohlhues L, Medin J, et al. RapidArc volumetric modulated therapy planning for prostate cancer patients. *Acta Oncol.* 2009;48:227–32.
- Yoo S, Wu Q.J, Lee W.R, et al. Radiotherapy treatment plans with RapidArc for prostate cancer involving seminal vesicles and lymph nodes. *Int J Radiat Oncol Biol Phys.* 2009;76:935–42.
- Ost P, Speleers B, De Meerleer G, et al. Volumetric arc therapy and intensity modulated radiotherapy for primary prostate radiotherapy with simultaneous integrated boost to intraprostatic lesion with 6 and 18 MV: A planning comparison study. *Int J Radiat Oncol Biol Phys.* 2011;79:920–6.

- Sze HC, Lee MC, Hung WM, et al. RapidArc radiotherapy planning for prostate cancer: single-arc and double-arc techniques vs. intensity modulated radiotherapy. *Med Dosim.* 2012;37: 87-91.
- Shaffer R, Morris W.J, Moiseenko V, et al. Volumetric modulated arc therapy and conventional intensity-modulated radiotherapy for simultaneous maximal intraprostatic boost: A planning comparison study. *Clin Oncol R Coll Radiol.* 2009;21:401–7.
- Kopp RW, Duff M, Catalfamo F et al. VMAT vs. 7-field-IMRT: assessing the dosimetric parameters of prostate cancer treatment with a 292-patient sample. *Med Dosim.* 2011; 36: 365–372.
- Bragg C, Windate K, Conway J. Clinical implications of the anisotropi canalytical algorithm for IMRT treatment planning and verification. *Radiother Oncol.* 2008;86:276–284.
- International Commission on Radiation Units and Measurements. ICRU Report 62. Prescribing, Recording, and Reporting Photon Beam Therapy (Supplement to ICRU Report 50). *J ICRU* 1999.
- Parker J, Kenyon R, Troxel D. Comparison of Interpolating Methods for Image Resampling. *IEEE Trans Med Imag.* 1983;2:31-39.
- Paddick I. A simple scoring ratio to index the conformity of radiosurgical treatment plans. Technical note. *J Neurosurg.* 2000; 93:219–22.
- Feuvret L, Noel G, Mazeron JJ, et al. Conformity index: A review. *Int J Radiat Oncol Biol Phys.* 2006; 64:333-342.
- Shapiro L G. Connected component labeling and adjacency graph con-struction. *Machine Intelligence and Pattern Recognition.* 1996;19:1-30.
- Lumia R. A New Three-Dimensional Connected Components Algorithm. *Compt Vis Graph Image Process.* 1983;22:207-220.
- Shibayama Y, Arimura H, Hirose TA et al. Investigation of interfractional shape variations based on statistical point distribution model for prostate cancer radiation therapy. *Med Phys.* 2017;44:1837-1845.
- McLaughlin PW, Wygoda A, Sahijdak W, et al. The effect of patient position and treatment technique in conformal treatment of prostate cancer. *Int J Radiat Oncol Biol Phys.*

1999;45:407-413.

Serrano NA, Kalman NS, Anscher MS. Reducing rectal injury in men receiving prostate cancer radiation therapy: current perspectives. *Cancer Manag Res.* 2017;9:339-350.

Boehmer D, Maingon P, Poortmans P, et al. Guidelines for primary radiotherapy of patients with prostate cancer. *Radiother Oncol* 2006;79:259–69.

Hayden AJ, Martin JM, Kneebone AB, et al. Australian & New Zealand faculty of radiation oncology genito - urinary group: 2010 consensus guidelines for definitive external beam radiotherapy for prostate carcinoma. *J Med Imaging Radiat Oncol* 2010;54:513–25.

Michalski J Purdy J, Bruner DW, et al. Radiation Therapy Oncology Group (RTOG) Report No. 0126, 2004.

Yu C X, “Intensity-modulated arc therapy with dynamic multileaf colli-mation: An alternative to tomotherapy,” *Phys Med Biol* 1995; 40:1435–1449.

Mayles P, Nahum A, Rosenwald JC. *Handbook of Radiotherapy Physics. Theory and Practice.* New York:Taylor & Francis Group, 2007.

Khan M. *Treatment Planning in Radiation Oncology.* Philadelphia: Lippincott Williams and Wilkins, 2007.

Mayles P, Nahum A, Rosenwald JC. *Handbook of Radiotherapy Physics. Theory and Practice.* New York: Taylor & Francis Group, 2007.

Perez CA, Purdy JA, Harms W, Gerber R, Graham MV, Matthews JW, Bosch W, Drzymala R, Emami B, Fox S, et al. Three-dimensional treatment planning and conformal radiation therapy: preliminary evaluation, *Radiother Oncol* 1995; 36:32-43.

Webb S, *Contemporary IMRT: Developing Physics and Clinical Implementation.* Institute of Physics Publishing, Bristol, 2005.

Bedford J, Treatment planning for volumetric modulated arc therapy. *Med Phys* 2009; 36: 5128–38.

Bzdusek K, et al. Development and evaluation of an efficient approach to volumetric arc therapy planning. *Med Phys* 2009; 36:2328–39.

Taqaddas A E. *Investigation of VMAT algorithms and Dosimetry.* AuthorHouse UK

Publishing, UK, 2011.

Chao K S C, Apisarnthanarax S, Ozyigit G. Practical Essentials of Intensity Modulated Radiation Therapy. Philadelphia: Lippincott Williams & Wilkins, 2005.



## Achievements

### **(1) 学術雑誌等（紀要・論文集等も含む） Academic Journals, etc.**

(査読あり Refereed)

- [1] **Tran Thi Thao Nguyen**, Hidetaka Arimura, Ryosuke Asamura, Taka-aki Hirose, Saiji Ohga, Jun-ichi Fukunaga. “Comparison of volumetric-modulated arc therapy and intensity-modulated radiation therapy prostate cancer plans accounting for cold spots”, Radiological Physics and Technology, Vol. 12, No. 2, p137-148.

### **(3) 国際会議における発表 Presentations in International Conferences**

(口頭発表 査読有り Oral presentation, Refereed)

- [2] ○**Nguyen Tran Thi Thao**, Hidetaka Arimura, Toshioh Fujibuchi, Hideki Hirata. “Investigation of dosimetric impacts of tissue heterogeneities in intracavitary brachytherapy for cervical cancer”, the 14<sup>th</sup> Asia-Oceania Congress of Medical Physics (AOCMP) & the 12<sup>th</sup> South East Asia Congress of Medical Physics (SEACOMP), Hochiminh City, Vietnam, October 23- 25, 2014.
- [3] ○**Nguyen Tran Thi Thao**, Hidetaka Arimura, Toshioh Fujibuchi, Hideki Hirata. “Evaluation of dose distributions in inhomogeneous phantom for intracavitary brachytherapy with high-dose rate <sup>192</sup>Ir source using Monte Carlo simulation”, Computer Assisted Radiology and Surgery (CARS), Fukuoka, Japan, June 25 -28 , 2014.
- [4] ○**Tran Thi Thao Nguyen**, Hidetaka Arimura, Yoshifumi Oku, Takashi Yoshiura. “Monte Carlo-based Assessment of Impacts of Heterogeneous Materials on Dose Distributions using Three-dimensional Gamma Analysis in Intracavitary Brachytherapy for Cervical Cancer”, the International Conference on Medical Physics (ICMP), Thailand, December 9-12, 2016.
- [5] ○**Tran Thi Thao Nguyen**, Hidetaka Arimura, Yoshifumi Oku, Takashi Yoshiura, Toshioh

Fujibuchi. “Impacts of inhomogeneous materials in intracavitary brachytherapy for cervical cancer”, the 10<sup>th</sup> Hope Meeting with Nobel Laureates, Yokohama, Japan, March 10-15, 2018.

- [6] ○**Tran Thi Thao Nguyen**, Hidetaka Arimura, Ryosuke Asamura, Taka-aki Hirose, Saiji Ohga, and Jun-ichi Fukunaga. “Computationally analysis of cold spots in dose distributions of VMAT plans for prostate cancer”, the 18<sup>th</sup> Asia-Oceania Congress of Medical Physics (AOCMP) & the 16<sup>th</sup> South East Asia Congress of Medical Physics (SEACOMP), Malaysia, Kuala Lumpur, November 11- 14, 2018.
- [7] Iwasaki Takahiro, Hidetaka Arimura, **Tran Thi Thao Nguyen**, Yoshifumi Oku, Takashi Yoshiura. “Monte Carlo-based Analysis of Impact of Tissue Heterogeneity on Dose Distributions in Cervical Cancer Intracavitary Brachytherapy”, the 22<sup>th</sup> International Conference on Medical Physics (ICMP), Thailand, December 9-12, 2016.

(ポスター発表 査読有り Poster presentation, Refereed)

- [8] ○**Tran Thi Thao Nguyen**, Hidetaka Arimura, Yoshifumi Oku, Toshioh Fujibuchi, Takahiro Nakamoto, Yusuke Shibayama, Hideki Hirata. “Impact of tissue inhomogeneity on dose distribution in CT-image-based brachytherapy for cervical cancer using Monte Carlo simulation”, the 15<sup>th</sup> International Congress of Radiation Research (ICRR), Kyoto, Japan, May 25-29, 2015.
- [9] ○**Tran Thi Thao Nguyen**, Hidetaka Arimura, Yoshifumi Oku, Takashi Yoshiura, Toshioh Fujibuchi. “Impacts of inhomogeneous materials in intracavitary brachytherapy for cervical cancer”, the 10<sup>th</sup> Hope Meeting with Nobel Laureates, Yokohama, Japan, March 10-15, 2018.

(ポスター展示 査読有り Poster exhibition, Refereed)

- [10] ○**Tran Thi Thao Nguyen**, Hidetaka Arimura, Yoshifumi Oku, Takahiro Nakamoto, Yusuke Shibayama, Takashi Yoshiura. “Three-Dimensional Dosimetric Gamma Analysis for Impacts of Tissue Inhomogeneity Using Monte Carlo Simulation in Intracavitary Brachytherapy for Cervix Carcinoma”, the 58<sup>th</sup> American Association Physicist in Medicine (AAPM), Washington DC, America, July 31 - August 3, 2016.
- [11] Yoshifumi Oku, Hidetaka Arimura, **Tran Thi Thao Nguyen**, Yoshiyuki Hiraki, Masahiko Toyota, Yasumasa Saigo, Takashi Yoshiura, Hideki Hirata. “ Robustness of adaptive intracavitary brachytherapy for uterine cervical cancer against interfractional location variations of organs and/or applicators”, the 112<sup>nd</sup> Scientific Meeting of the Japan Society of Medical Physics, Okinawa, Japan, September 8-10, 2017.
- [12] Takahiro Iwasaki, Hidetaka Arimura, **Tran Thi Thao Nguyen**, Yoshifumi Oku, Takashi Yoshiura. “Monte Carlo-based Gamma Analysis of Impact of Tissue Heterogeneity on Dose distributions in Cervical Cancer Intracavitary Brachytherapy”, International Conference on Medical Physics 2016 (ICMP2016), Thailand, December 9-12, 2016.
- [13] **Tran Thi Thao Nguyen**, Hidetaka Arimura, Yoshifumi Oku, Takashi Yoshiura, Toshioh Fujibuchi. “Impacts of inhomogeneous materials in intracavitary brachytherapy for cervical cancer”, the 10<sup>th</sup> Hope Meeting with Nobel Laureates, Yokohama, Japan, March 10-15, 2018.

#### **(4) 国内学会・シンポジウム等における発表 Presentations in Domestic Conferences**

(口頭発表 査読有り Oral presentation, Refereed)

- [14] ○**Tran Thi Thao Nguyen**, Hidetaka Arimura, Toshioh Fujibuchi, Hideki Hirata. “Investigation of variation of dose distribution in inhomogeneous phantom for intracavitary brachytherapy with HDR <sup>192</sup>Ir using Monte Carlo simulation”, the 107<sup>th</sup> Scientific Meeting of the Japan Society of Medical Physics ,Yokohama, Japan, April 10-

13, 2014.

- [15] ○**Tran Thi Thao Nguyen**, Hidetaka Arimura, Yoshifumi Oku, Takahiro Iwasaki, Takashi Yoshiura. “Monte Carlo Simulations Analysis of Dosimetric Impacts of Titanium Applicator and Tissue Inhomogeneity of Cervical Intracavitary Brachytherapy”, the 113<sup>th</sup> Scientific Meeting of the Japan Society of Medical Physics, Yokohama, Japan, April 13-16, 2017.
- [16] ○**Tran Thi Thao Nguyen**, Hidetaka Arimura, Yoshifumi Oku, Takahiro Iwasaki, Takahiro Nakamoto, Takashi Yoshiura. “Brachytherapy for Treatment of Cervical Cancer”, the 9<sup>th</sup> Vietnamese-Japanese Student’s Scientific Exchange Meeting, Fukuoka, Japan, September 17, 2016.
- [17] ○**Tran Thi Thao Nguyen**, Hidetaka Arimura, Ryosuke Asamura, Mazen Soufi, Saiji Ohga, Hiroshi Honda, Tomonari Sasaki. “Dosimetric analysis of cold spots in intensity-modulated radiation therapy for the treatment of prostate cancer”, 医用画像情報学会 (第 180 回), Gifu, Japan, January 27, 2018.
- [18] ○**Tran Thi Thao Nguyen**, Hidetaka Arimura, Yoshifumi Oku, Takahiro Iwasaki, Takahiro Nakamoto, Toshioh Fujibuchi, Takashi Yoshiura. “Effect of a brachytherapy applicator and tissue heterogeneity on dose distributions using Monte Carlo simulations for cervical cancer”, the 115<sup>th</sup> Scientific Meeting of the Japan Society of Medical Physics, Yokohama, Japan, April 12-15, 2018.
- [19] Takahiro Iwasaki, Hidetaka Arimura, **Tran Thi Thao Nguyen**, Yoshifumi Oku, Takashi Yoshiura, Hideki Hirata. “子宮頸癌腔内照射の 3 次元治療計画におけるモンテカルロシミュレーションを用いた線量分布への組織不均一の影響の解析”, 九州放射線医療技術学術大会, 宮崎, 日本, 10 月 31 日-11 月 1 日, 2015 年.
- [20] Takahiro Iwasaki, Hidetaka Arimura, **Tran Thi Thao Nguyen**, Yoshifumi Oku, Takashi Yoshiura, Hideki Hirata. “Analysis of influence of tissue heterogeneity on dose

distribution in intracavitary treatment of cervix carcinoma on 3D treatment planning”, the 111<sup>th</sup> Scientific Meeting of the Japan Society of Medical Physics, Yokohama, Japan, April 14<sup>th</sup> -17<sup>th</sup>, 2016.

(口頭発表 査読なし Oral presentation, No Refereed)

- [21] ○**Tran Thi Thao Nguyen**, Hidetaka Arimura. “Are you satisfied with studying in japan”, International Symposium, the 111<sup>th</sup> Scientific Meeting of the Japan Society of Medical Physics, Yokohama, April 14<sup>th</sup> -17<sup>th</sup>, 2016.
- [22] ○**Tran Thi Thao Nguyen**, Alexandra Rose McNeil, Yoshihide Tokunou, Lakhwinder Singh, Nithi Atthi, Nur Ardiyana Binti Rejab, Orkun Coruh, Wen Wei Liu, Geng Tian, “How dose public perception affect science”, the 10<sup>th</sup> Hope Meeting with Nobel Laureates, Yokohama, Japan, March 10-15, 2018.
- [23] ○**Tran Thi Thao Nguyen**, Chau Van Tao, et al. “Designing a software to calculate dose rate and simulate dose distribution for condensed cylinder gamma sources”, High Energy Accelerator Research Organization (KEK), Tsukuba, Japan, March 2014.
- [24] ○**Tran Thi Thao Nguyen**, Hidetaka Arimura, et al. “Usefulness of Monte Carlo simulation in brachytherapy”, the 55<sup>th</sup> Graduated Students’ Meeting, Kyushu University, Fukuoka, May 2014.

#### **(5) 特許等 Patents, ect.**

None

#### **(6) その他（受賞歴等） Others (Awards, etc.)**

- [25] 2014. 03: **Invited as Young Lady Investigator** for High Energy Accelerator Research Organization at Tsukuba, Japan.

- [26] 2014. 10. 23 ~ 25: **Best Oral Presentation International Award**, at the 14<sup>th</sup> Asia-Oceania Congress of Medical Physics & the 12<sup>th</sup> South East Asia Congress of Medical Physics (SEACOMP), Vietnam.
- [27] 2013. 04 ~ 2015. 09: Japanese Government – (Monbukagakusho: MEXT) Scholarship.
- [28] 2015. 10 ~ 2016. 03: Sato Yo International Scholarship Foundation.
- [29] 2016.04 ~2019.03: 日本学術振興会特別研究員(DC1)
- [30] 2016. 09. 17: **Best Oral Presentation Award**, at the Vietnamese-Japanese Students' Scientific Exchange Meeting (VJSE-2016), Japan.
- [31] 2018.03. 23 ~ 15: **Selected student** for the 10th Hope meeting with **Nobel Laureates**.
- [32] 2012. 10~12: **Studying Abroad** in Institute of Nuclear Techniques of the Budapest University Technology and Economic and by MVM Paks Nuclear Power Plant Ltd. (Hungarian-Vietnamese Nuclear Education and Training program HUVINETT), Budapest, **Hungary**.
- [33] 2018. 11. 11 ~ 14: **Best Oral Presentation International Award**, at the 18<sup>th</sup> Asia-Oceania Congress of Medical Physics & the 16<sup>th</sup> South East Asia Congress of Medical Physics (SEACOMP), Malaysia.